Inorganic Chemistry

Article

pubs.acs.org/IC

Allosteric Effects in Binuclear Homo- and Heterometallic Triple-Stranded Lanthanide Podates

Patrick E. Ryan,[§] Gabriel Canard,*[,§,⊥] Sylvain Koeller,[§] Bernard Bocquet,[§] and Claude Piguet*[,§]

[§]Department of Inorganic, Analytical and Applied Chemistry, University of Geneva, 30 quai E. Ansermet, CH-1211 Geneva 4, Switzerland

[⊥]Faculty of Sciences de Marseille Saint Jérôme, Avenue escadrille Normandie-Niemen, F-13397 Marseille Cedex 20, France

Supporting Information

ABSTRACT: This work illustrates a simple approach for deciphering and exploiting the various free energy contributions to the global complexation process leading to the binuclear triple-stranded podates $[Ln_2(\mathbf{L9})]^{6+}$ (Ln is a trivalent lanthanide). Despite the larger microscopic affinities exhibited by the binding sites for small Ln^{3+}, the stability constants measured for $[Ln_2(\mathbf{L9})]^{6+}$ decrease along the lanthanide series; a phenomenon which can be ascribed to the severe enthalpic penalty accompanying the intramolecular cyclization around small Ln(III), combined with increasing anticooperative allosteric interligand interactions. Altogether, the microscopic thermodynamic characteristics predict $\beta_{1,1,1}^{La,Lu,L9}/\beta_{1,1,1}^{Lu,La,L9} = 145$ for the ratio of the formation constants of the target heterobimetallic $[LaLu(\mathbf{L9})]^{6+}$ and $[LuLa(\mathbf{L9})]^{6+}$ microspecies, a value in line with the quantitative preparation (>90%) of $[LaLu(\mathbf{L9})]^{6+}$ at millimolar concentrations. Preliminary NMR titrations indeed confirm the rare thermodynamic programming of a pure heterometallic f-f′ complex.

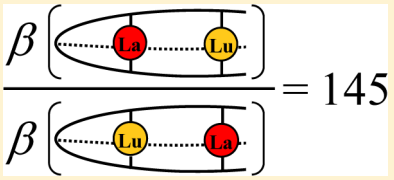

INTRODUCTION

The stereochemical preference of numerous divalent and trivalent d-block cations M^{z+} (z = 2, 3) for octahedral geometry, combined with the considerable chelate effect brought by rigid bidentate 2,2′-bipyridine (**L1**)[1] result in the systematic formation of stable six-coordinated D_3-helical $[M(\mathbf{L1})_3]^{z+}$ complexes with predetermined structures (Scheme 1).[2] Improved structural control and stabilities are achieved by the connection of the bidentate binding units to a covalent tripod in **L2**,[3] a strategy which has been further exploited for the selective complexation of different cations in the C_3-helical $[FeHg(\mathbf{L3})]^{4+}$ complex,[4] and for the programming of redox-induced intramolecular metal translocation in $[Fe(\mathbf{L4})]^{2/3+}$.[5] A strict geometrical analogy can be drawn for trivalent 4f-cations, Ln^{3+}, whose preference for nine-coordination is satisfied by the complexation of three rigid terdentate 2,2′;6′,2″-terpyridine ligands in the D_3-helical $[Ln(\mathbf{L5})_3]^{3+}$ complexes.[6] Because of the bent meridional tercoordination of **L5** to Ln(III), the connection of three such terpyridine units to a covalent tripod in **L6** induces severe geometrical limitations for the preparation of the putative mononuclear nine-coordinated podates $[Ln(\mathbf{L6})]^{3+}$, a challenge which remains unsolved despite the exploration of the complexation properties of **L6** with Ln(III) = La, Pr, Eu, and Lu.[7]

In this context, the extended terdentate aromatic ligand **L7** provides three crucial advantages over **L5** for coordinating lanthanides: (1) the stacked benzimidazole side arms control the size of the metallic cavity in the target triple-helical nine-coordinate complexes $[Ln(\mathbf{L7})_3]^{3+}$,[8] (2) the associated selectivity can be tuned by a judicious choice of the substituents bound to the noncoordinating nitrogen atoms of the benzimidazole rings,[9] and (3) the connection with a covalent tripod requires straightforward synthetic transformations of terminal phenyl rings in **L7**, instead of more demanding modifications of pyridine rings in **L5**.[10] Consequently, the tripodal ligand **L8** represents a rare case, in which three bent terdentate polyaromatic *N*-heterocyclic binding units are coordinated to a single trivalent lanthanide to give stable mononuclear $[Ln(\mathbf{L8})]^{3+}$ podates.[11] Despite the promising selectivity brought by the variable chelate effect operating along the lanthanide series for this neutral N_9 ligand,[11] no attempt for exploiting this strategy in the design of binuclear heterometallic podates has been considered, while remarkable reports describe the systematic use of NNO or NOO binding units for the complexation of lanthanide cations in related mononuclear nine-coordinate podates.[12] In this contribution, we report on (i) the synthesis of an unprecedented (to the best of our knowledge) compartmental bis-nine-coordinate podate **L9** and (ii) its reactivity with Ln(III) along the lanthanide series with the ultimate goal of producing pure heterobimetallic 4f-4f′ microspecies under thermodynamic control.

RESULTS AND DISCUSSION

Synthesis and Characterization of the Podand L9 and Its Complexes $[Ln_2(L9)](CF_3SO_3)_6$ (Ln = La, Lu). The ligand **L9** is prepared in 30 synthetic steps from the commercially available compounds **1**, **3**, **7**, and **17** according to a strategy previously developed for **L8** (Scheme 2).[11] Two successive amidation reactions produce the unsymmetrical bis-*o*-nitroareneamide key intermediate **11**, which undergoes a reducing cyclization to give **12**. Four successive tedious, but efficient reactions introduce a terminal nucleophilic thiol group in **16**, which is deprotonated and coupled under anaerobic conditions

Received: July 25, 2012
Published: September 4, 2012

 © 2012 American Chemical Society dx.doi.org/10.1021/ic301631n | *Inorg. Chem.* 2012, 51, 10012−10024

Scheme 1. Chemical Structures of the Ligands L1−L9 with Numbering Scheme for ^{1}H NMR Studies

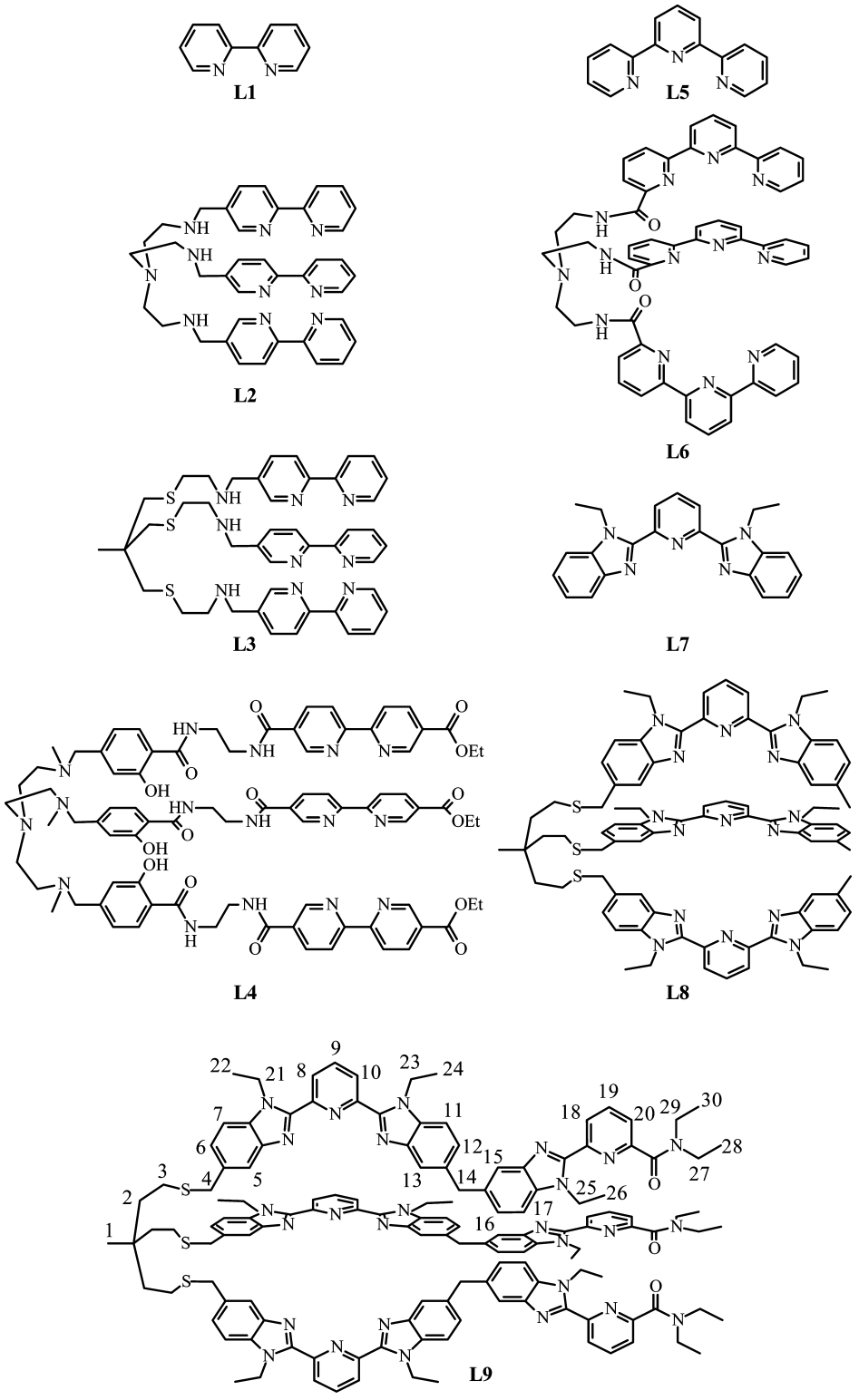

with the electrophilic trichloride **21**[13] to afford **L9** in acceptable yield.

The ^{1}H NMR spectrum of **L9** displays 30 signals (Supporting Information, Table S1) in agreement with the existence of a 3-fold axis, completed with three vertical symmetry planes (i.e., C_{3v} point group) responsible for the detection of enantiotopic protons for the methylene groups of each strand (Figure 1a).

Reaction of **L9** (1 equiv.) with $Ln(CF_3SO_3)_3{\cdot}xH_2O$ (Ln = La, Lu; x = 1−3; 2 equiv.) in acetonitrile followed by slow diffusion of diethylether gave $[La_2(\mathbf{L9})](CF_3SO_3)_6{\cdot}16H_2O$ and $[Lu_2(\mathbf{L9})](CF_3SO_3)_6{\cdot}12H_2O$ in fair yield (40−70%). The associated ^{1}H NMR spectra still display 30 signals in line with the regular wrapping of the three strands around the two metals defining the 3-fold axis, but the diastereotopic methylene protons (AB spin systems) point to the loss of the symmetry planes

dx.doi.org/10.1021/ic301631n | Inorg. Chem. 2012, 51, 10012−10024

Scheme 2. Synthesis of the Ligand L9

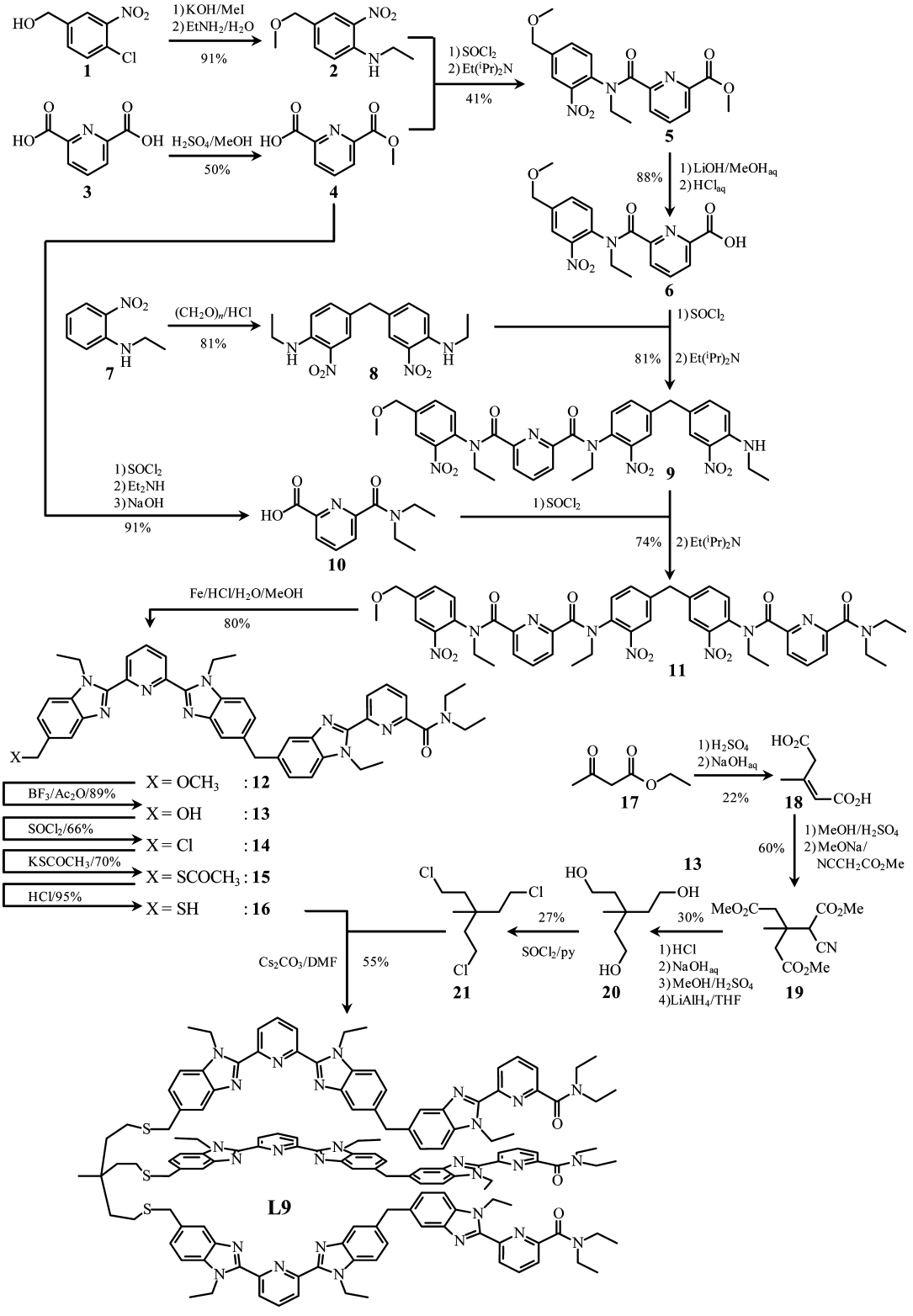

induced by the helical arrangement of the ligand strands (i.e., C_3 point group, Figure 1b,c). The complexation process affects all ^{1}H NMR chemical shifts, with a special emphasis on the considerable upfield shifts displayed by the singlets assigned to the protons H5 ($\Delta\delta$ = −1.54 to −1.75 ppm), H13 ($\Delta\delta$ = −1.76 to −2.28 ppm) and H15 ($\Delta\delta$ = −1.71 to −2.23 ppm, Figure 1b,c and Supporting Information, Table S1). This behavior is diagnostic for the formation of a triple-helical arrangement of the bound ribbons in the binuclear complexes, which puts these protons in the shielding region of the benzimidazole rings of the adjacent strands[14] as previously reported for related protons in the mononuclear diamagnetic triple-helical podates $[Ln(\mathbf{L8})]^{3+}$ ($\Delta\delta$ = −0.83 to −1.46 ppm, Ln = La, Y, Lu).[11]

dx.doi.org/10.1021/ic301631n | Inorg. Chem. 2012, 51, 10012−10024

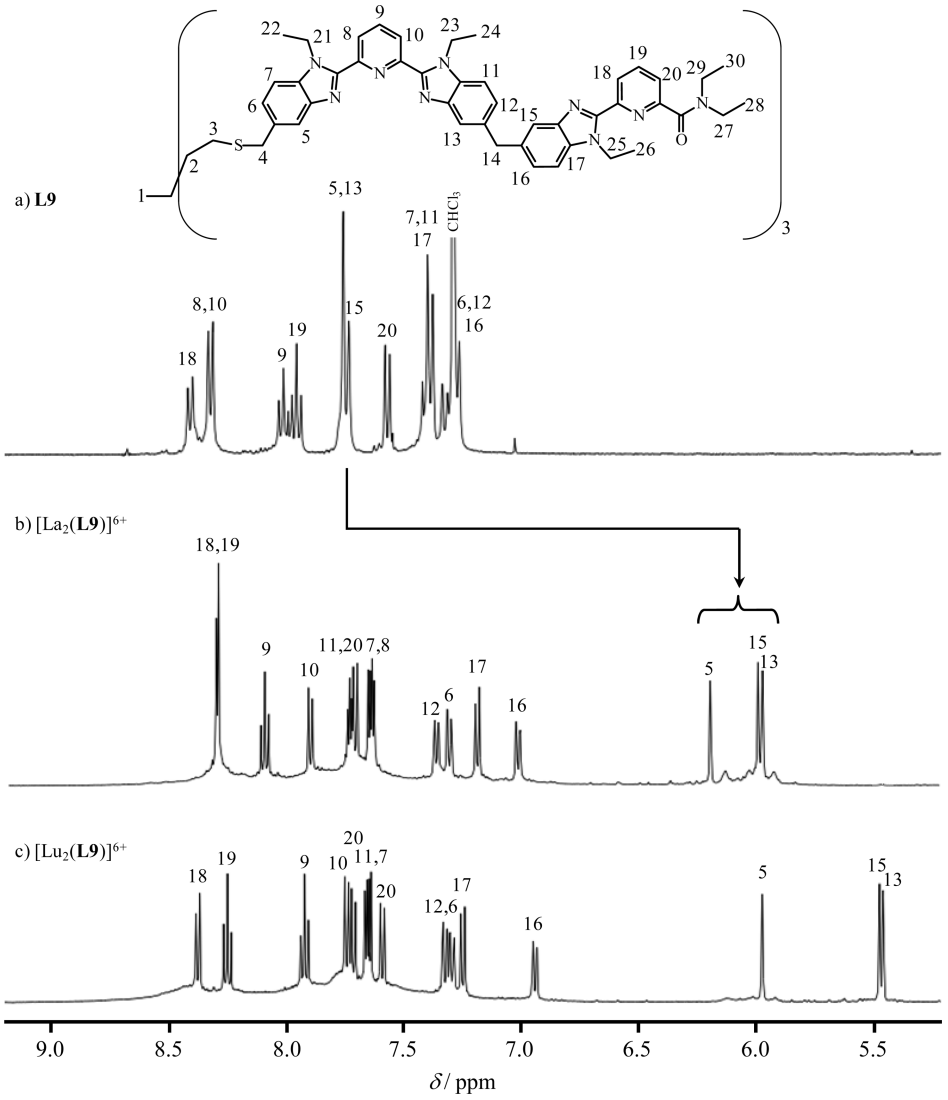

Figure 1. Aromatic parts in the ^{1}H NMR spectra of (a) the ligand **L9** ($CDCl_3$) and its complexes (b) $[La_2(\mathbf{L9})]^{6+}$ and (c) $[Lu_2(\mathbf{L9})]^{6+}$ (CD_3CN, 298 K).

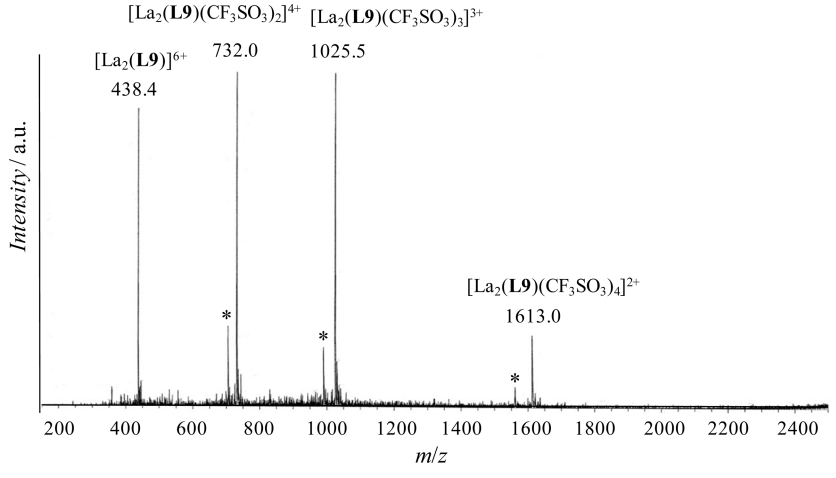

Figure 2. ESI-MS spectrum of $[La_2(\mathbf{L9})]^{6+}$ in CH_3CN/CH_2Cl_2 (9:1) at 298 K. The series of peaks marked with an asterisk, *, corresponds to $[La_2(\mathbf{L9})(HCOO)(CF_3SO_3)_n]^{(5-n)+}$ (n = 1−3), which result from a minor contamination of the sprayer with formic acid.

Electrospray ionization mass spectrometry (ESI-MS) spectra recorded in acetonitrile/dichloromethane for $[Ln_2(\mathbf{L9})](CF_3SO_3)_6$ (Ln = La, Eu, Lu) unambiguously confirm the existence of the binuclear complexes in solution with the detection of $[Ln_2(\mathbf{L9})]^{6+}$ together with its adducts $[Ln_2(L9)(CF_3SO_3)_n]^{(6-n)+}$ (Figure 2). Upon stepwise titrations of **L9** (0.2 mM) with $Ln(CF_3SO_3)_3 \cdot xH_2O$, additional ESI-MS signals can be assigned to the formation of the mononuclear precursors

dx.doi.org/10.1021/ic301631n | Inorg. Chem. 2012, 51, 10012−10024

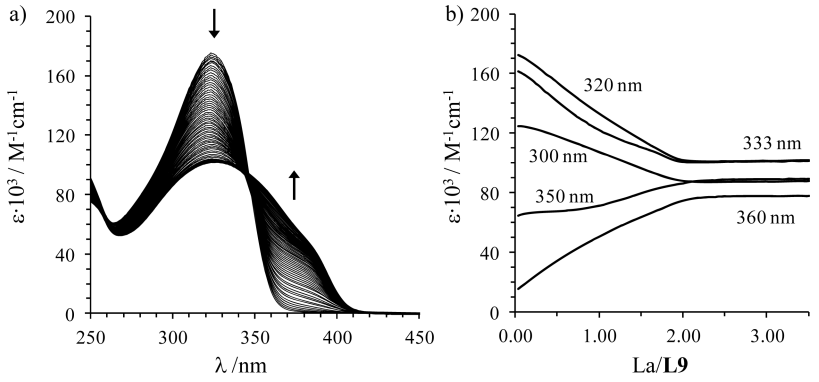

Figure 3. (a) Variation of absorption spectra and (b) corresponding variation of the molar extinctions at five different wavelengths observed for the spectrophotometric titration of **L9** ($7\cdot10^{-5}$ M) with $La(CF_3SO_3)_3\cdot H_2O$ (acetonitrile/dichloromethane (9:1) + 10^{-2} M NBu_4ClO_4, 298 K).

$[Ln(\mathbf{L9})]^{3+}$ in default of metal. The intensities of the latter signals culminate around $|Ln|_{tot}/|\mathbf{L9}|_{tot} \approx 1$, followed by their decrease and the growing up of the peaks produced by $[Ln_2(\mathbf{L9})]^{6+}$ (Supporting Information, Tables S2−S4). No other significant cationic species could be detected and the complexation process can be summarized with the macroscopic equilibria 1 and 2

$$Ln^{3+} + \mathbf{L9} \rightleftharpoons [Ln(\mathbf{L9})]^{3+} \qquad \beta_{1,1}^{Ln,\mathbf{L9}} \qquad (1)$$

$$2Ln^{3+} + \mathbf{L9} \rightleftharpoons [Ln_2(\mathbf{L9})]^{6+} \qquad \beta_{2,1}^{Ln,\mathbf{L9}} \qquad (2)$$

Thermodynamic Behavior of the Complexes $[Ln_2(L9)](CF_3SO_3)_6$ (Ln = La, Eu, Lu). The thermodynamic stability macroconstants $\beta_{m,1}^{Ln,\mathbf{L9}}$ (eqs 1−2) were obtained by spectrophotometric titrations of **L9** with $[Ln(CF_3SO_3)_3]\cdot xH_2O$ (Ln = La, Eu, Lu) because the trans-trans → cis-cis conformational change of the benzimidazole-pyridine scaffolds accompanying the complexation process induces some significant differences in the electronic structure,[15] which are easily monitored in the UV part of the absorption spectra (Figure 3a).[16]

The lack of isosbestic points suggests the existence of at least three absorbing species in solution, whereas the two smooth end points observed for $|Ln|_{tot}/|\mathbf{L9}|_{tot}$ = 1.0 and 2.0 (Figure 3b) confirm the operation of equilibria 1 and 2. The spectrophotometric data were satisfyingly fitted by using nonlinear least-squares techniques[17] to give the cumulative formation constants collected in Table 1 (entries 1−2).

One immediately notices the operation of an antielectrostatic trend (i.e., $\beta_{m,1}^{La,\mathbf{L9}} > \beta_{m,1}^{Eu,\mathbf{L9}} > \beta_{m,1}^{Lu,\mathbf{L9}}$) leading to a considerable destabilization of the complexes $[Ln(\mathbf{L9})]^{3+}$ and $[Ln_2(\mathbf{L9})]^{6+}$ for the smaller lanthanide cations, the origin of which can be approached by using the site-binding model.[18] Using the van't Hoff equation with a standard concentration for the reference state of c^θ = 1 M,[19] the thermodynamic formation macroconstants $\beta_{m,1}^{Ln,\mathbf{L9}}$ (eqs 3 and 4) can be written as the weighted products of a limited set of "easily" interpretable thermodynamic describers.[18]

$$\begin{aligned}\beta_{1,1}^{Ln,\mathbf{L9}} &= e^{-(\Delta G_{1,1}^{Ln,\mathbf{L9}}/RT)} \\ &= \omega_{1,1,N3}^{chiral}\omega_{1,1,N3}^{Ln,\mathbf{L9}}(f_{N3}^{Ln})^3(EM_{prox}^{Ln})^2(e^{-\Delta E_{Ln}^{N3,N3}/RT})^3 \\ &\quad + \omega_{1,1,N2O}^{chiral}\omega_{1,1,N2O}^{Ln,\mathbf{L9}}(f_{N2O}^{Ln})^3(EM_{dist}^{Ln})^2 \\ &\quad (e^{-\Delta E_{Ln}^{N2O,N2O}/RT})^3 \end{aligned} \qquad (3)$$

Table 1. Cumulative Thermodynamic Formation Constants $\log(\beta_{m,1}^{Ln,\mathbf{L9}})$, Associated Intermolecular Microscopic Affinities,[a] Intramolecular Microscopic Affinities,[b], Intermetallic[c] Interactions, and Interligand[d] Interactions Obtained for $[Ln_2(L9)]^{6+}$ (Ln = La, Eu, Lu; CH_3CN/CH_2Cl_2 (9:1) + 10^{-2} M NBu_4ClO_4, 298 K)

	metal		
	La	Eu	Lu
$\log(\beta_{1,1}^{Ln,\mathbf{L9}})$	8.89(4)	6.41(9)	5.57(1)
$\log(\beta_{2,1}^{Ln,\mathbf{L9}})$	15.47(5)	12.80(8)	10.82(1)
$\log(f_{N3}^{Ln}))$	6.9(2)	7.1(1)	9.63(2)
$\Delta G_{inter}^{Ln,N3}$/kJ·mol^{-1}	−39.1(9)	−40.5(4)	−54.9(1)
$\log(f_{N2O}^{Ln})$	3.7(2)	8.0(1)	9.05(2)
$\Delta G_{inter}^{Ln,N2O}$/kJ·mol^{-1}	−21(1)	−45.6(4)	−51.6(1)
$\log(EM_{prox}^{Ln})$	−3.8(5)	−6.6(2)	−8.0(4)
$\Delta G_{intra,prox}^{Ln,N3}$/kJ·mol^{-1}	−18(3)	−3(1)	−9(2)
$\Delta G_{intra,dist}^{Ln,N2O}$/kJ·mol^{-1}	4(3)	−5(1)	−3(2)
$\Delta G_{intra,dist\text{-}n}^{Ln,N2O}$/kJ·mol^{-1}	1(3)	−8(1)	−6(2)
$\log(u_{Ln}^{N3,N3})$	−1.7(3)	−0.9(1)	−2.3(2)
$\Delta E_{Ln}^{N3,N3}$/kJ·mol^{-1}	10(2)	5(1)	13(1)
$\log(u_{Ln}^{N2O,N2O})$	0.8(3)	−1.3(1)	−1.7(2)
$\Delta E_{Ln}^{N2O,N2O}$/kJ·mol^{-1}	−4(2)	8(1)	10(1)
$\log(u^{Ln,Ln})$	0(2)	−0.9(8)	−3(1)
$\Delta E^{Ln,Ln}$/kJ·mol^{-1}	−2(10)	5(4)	16(8)

[a] $\Delta G_{inter}^{Ln,N3} = -RT\ln(f_{N3}^{Ln})$ and $\Delta G_{inter}^{Ln,N2O} = -RT\ln(f_{N2O}^{Ln})$. [b] $\Delta G_{intra,prox}^{Ln,N3} = -RT\ln(EM_{prox}^{Ln}f_{N3}^{Ln})$, $\Delta G_{intra,dist}^{Ln,N2O} = -RT\ln(0.29EM_{prox}^{Ln}f_{N2O}^{Ln})$, and $\Delta G_{intra,dist\text{-}n}^{Ln,N2O} = -RT\ln(0.69EM_{prox}^{Ln}f_{N2O}^{Ln})$. [c] $\Delta E^{Ln,Ln} = -RT\ln(u^{Ln,Ln})$. [d] $\Delta E_{Ln}^{N3,N3} = -RT\ln(u_{Ln}^{N3,N3}$ and $\Delta E_{Ln}^{N2O,N2O} = -RT\ln(u_{LN}^{N2O,N2O})$.

$$\begin{aligned}\beta_{2,1}^{Ln,\mathbf{L9}} &= e^{-(\Delta G_{2,1}^{Ln,\mathbf{L9}}/RT)} \\ &= \omega_{2,1}^{chiral}\omega_{2,1}^{Ln,\mathbf{L9}}(f_{N3}^{Ln})^3(f_{N2O}^{Ln})^3(EM_{prox}^{Ln})^2(EM_{dist\text{-}n}^{Ln})^2 \\ &\quad (e^{-\Delta E_{Ln}^{N3,N3}/RT})^3\cdot(e^{-\Delta E_{Ln}^{N2O,N2O}/RT})^3(e^{-\Delta E^{Ln,Ln}/RT}) \end{aligned} \qquad (4)$$

The first contributions $\Delta G_{stat}^{Ln,\mathbf{L9}} = -RT\ln(\omega_{m,n}^{chiral}\cdot\omega_{m,n}^{Ln,\mathbf{L9}})$ correspond to the changes in rotational entropy occurring when the reactants are transformed into products. It can be computed by using the symmetry numbers (σ^{ext}, σ^{int}, and σ^{chiral}) controlling the statistical factors of the assembly $\omega_{m,n}^{chiral}\cdot\omega_{m,n}^{Ln,\mathbf{L9}}$, as soon as the point groups of the various partners are at hand.[20] As a working example, let us begin with the first part of eq 3 which models the microconstant for the formation of the *proximal*-$[Ln(\mathbf{L9})]^{3+}$ microspecies, where the Ln^{3+} cation occupies the internal nine-coordinate cavity produced by the three wrapped

dx.doi.org/10.1021/ic301631n | *Inorg. Chem.* 2012, 51, 10012−10024

terdentate N_3 binding units (Figure 4a). In this case $\omega_{1,1,N3}^{chiral}\cdot\omega_{1,1,N3}^{Ln,L9}$ =12 (Supporting Information, Figure S1a),

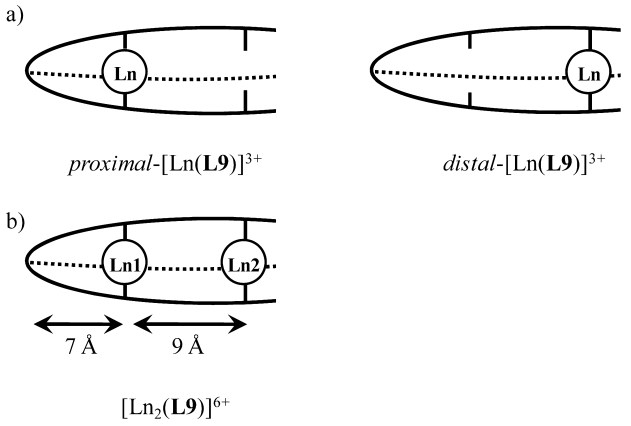

Figure 4. Schematic structural representations of the microspecies contributing to (a) $[Ln(\mathbf{L9})]^{3+}$ and (b) $[Ln_2(\mathbf{L9})]^{6+}$ with pertinent distances taken from the crystal structures of $[Eu(\mathbf{L8})]^{3+}$ 11 and *HHH*-$[LaTb(\mathbf{L10})_3]^{6+}$.[24]

whereas the second term $\Delta G_{inter}^{Ln,N3} = -RT\sum_{i=1}^{3}(f_{N3}^{Ln})$ represents the sum of the free energies of metal-N_3 binding unit connections, which includes the desolvation/solvation processes accompanying the complexation process.[21] However, among the three Ln-N_3 binding connections occurring in *proximal*-$[Ln(\mathbf{L9})]^{3+}$, only one is intermolecular and corresponds to the association of two partners freely moving and statistically dispersed in the condensed phase. The two remaining Ln-N_3 coordination events are intramolecular, and the associated free energy change $\Delta G_{intra}^{Ln,N3} = -RT\ \ln(EM_{prox}^{Ln}f_{N3}^{Ln})$ additionally depends on the effective molarities (EM_{prox}^{Ln}) of the interacting partners imposed by the reduced motion of the ligand strands.[22] Finally, $\Delta E_{Ln}^{N3,N3} = -RT\ \ln(u_{Ln}^{N3,N3})$ corresponds to the homocomponent interaction produced by the close location of two N_3 binding units connected to the same metal. This approach can be repeated for the alternative *distal*-$[Ln(\mathbf{L9})]^{3+}$ microspecies (second part of eq 3), where Ln^{3+} occupies the remote nine-coordinate cavity produced by the three terminal terdentate N_2O binding units (Figure 4b). Since the binuclear complex $[Ln_2(\mathbf{L9})]^{6+}$ exists as a single microspecies (Figure 4c), its thermodynamic modeling is much simpler with $\Delta E^{Ln,Ln} = -RT\ln(u^{Ln,Ln})$ standing for the two metals bound in the adjacent cavities (eq 4). If we roughly assume that the chains of atoms constituting the chelate rings in $[Ln_2(\mathbf{L9})]^{6+}$ behave as freely joint chains, Kuhn's theory[23] predicts that $EM \sim d^{-3/2}$, where d is the distance separating the two connecting points involved in the intramolecular process.

Taking simplified representations for the various $[Ln_m(\mathbf{L9})]^{3m+}$ complexes (Figure 4) with pertinent distances measured in the crystal structures of $[Eu(\mathbf{L8})]^{3+}$[11] and *HHH*-$[LaTb(\mathbf{L10})_3]^{6+}$ (see Scheme 3 for the chemical structure of this ligand),[24] we calculate $L^{N3,N3} = 2\times 7 = 14$ Å for the approximate end-to-end chain length of the chelate ring controlling EM_{prox}^{Ln} in *proximal*-$[Ln(\mathbf{L9})]^{3+}$ (Figure 4a), and $L^{N2O,N2O} = (2\times 7 + 2\times 9) = 32$ Å for EM_{dist}^{Ln} in *distal*-$[Ln(\mathbf{L9})]^{3+}$ (Figure 4b). Kuhn's theory then yields $EM_{dist}^{Ln}/EM_{prox}^{Ln} = (L^{N2O,N2O}/L^{N3,N3})^{-3/2} = 0.29$, and this approach can be repeated for the binuclear podate $[Ln_2(\mathbf{L9})]^{6+}$ where the missing effective molarity $EM_{dist\text{-}n}^{Ln}$ characterizing the intramolecular ring closure around Ln2 in presence of Ln1 is given by $EM_{dist\text{-}n}^{Ln}/EM_{prox}^{Ln} = (L_n^{N2O,N2O}/L^{N3,N3})^{-3/2} = (2\times 9/14)^{-3/2} = 0.69$ (Figure 4c). Introducing these ratios together with the statistical factors (computed in Supporting Information, Figure S1) into eqs 3−4 eventually yields eqs 5 and 6, in which only six microscopic thermodynamic describers are involved.

Scheme 3. Chemical Structures of the Ligands L10−L12

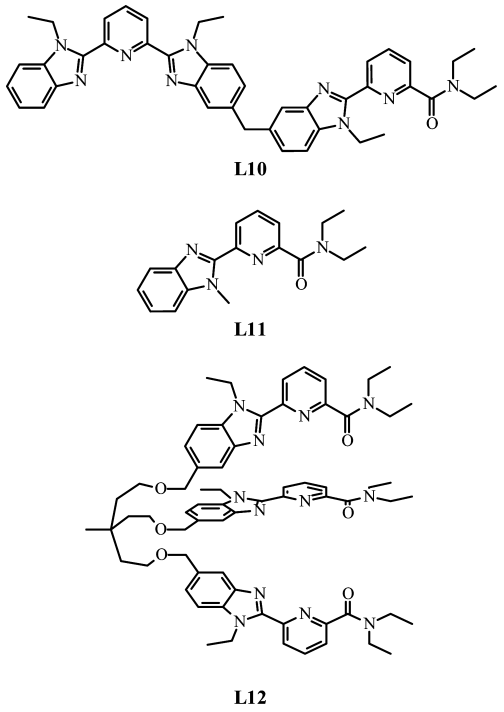

$$\beta_{1,1}^{Ln,\mathbf{L9}} = 12(EM_{prox}^{Ln})^2[(f_{N3}^{Ln})^3(u_{Ln}^{N3,N3})^3 + (f_{N2O}^{Ln})^3(0.29)^2 (u_{Ln}^{N2O,N2O})^3] \quad (5)$$

$$\beta_{2,1}^{Ln,\mathbf{L9}} = 72(f_{N3}^{Ln})^3(f_{N2O}^{Ln})^3(EM_{prox}^{Ln})^4(0.69)^2(u_{Ln}^{N3,N3})^3 (u_{Ln}^{N2O,N2O})^3(u^{Ln,Ln}) \quad (6)$$

Additional thermodynamic information is gained from the spectrophotometric titrations of the ligands **L7** and **L11** (equilibria 7, n = 1−3), each mirroring one specific terdentate binding site (N_3 and N_2O, respectively) found in **L9**, and of the podands **L8** and **L12** (equilibrium 8), each mirroring one specific nine-coordinate cavity found in **L9** (N_9 and N_6O_3, respectively), with $[Ln(CF_3SO_3)_3]\cdot xH_2O$ (Ln = La, Eu, Lu) in the same experimental conditions (Supporting Information, Table S5).

$$Ln^{3+} + n\mathbf{Lk} \rightleftharpoons [Ln(\mathbf{Lk})_n]^{3+} \qquad \beta_{1,n}^{Ln,\mathbf{Lk}} \quad (7)$$

$$Ln^{3+} + \mathbf{Lk} \rightleftharpoons [Ln(\mathbf{Lk})]^{3+} \qquad \beta_{1,n}^{Ln,\mathbf{Lk}} \quad (8)$$

Each thermodynamic formation constant is modeled with the site binding model (Supporting Information, Figures S2−S4), and the resulting set of 10 stability constants (eqs 5, 6, and Supporting Information, eqs S1−S8) can be satisfyingly fitted by using nonlinear least-squares techniques (Agreement Factors[25] $AF_{Ln} \leq 0.075$, Supporting Information, Table S5, and Figure S5) to give the microscopic thermodynamic describers collected in Table 1.

The intermolecular microscopic affinities of the binding sites for the entering metal provide the major driving forces to the complexation process leading to $[Ln_2(\mathbf{L9})]^{6+}$ (Table 1, entries

dx.doi.org/10.1021/ic301631n | Inorg. Chem. 2012, 51, 10012−10024

3−6 and Figure 5a). In line with the well-known electrostatic effect, the free energy of intermolecular connection increases

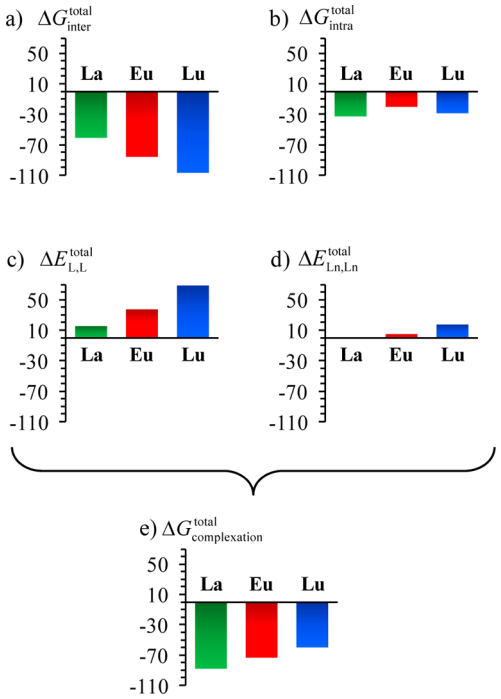

Figure 5. Representation of the thermodynamic contributions in kJ/mol corresponding to (a) intermolecular and (b) intramolecular Ln-ligand connections, and (c) interligand and (d) intermetallic interactions responsible for the global complexation process leading to $[Ln_2(\mathbf{L9})]^{6+}$ (Ln = La, Eu, Lu; CH_3CN/CH_2Cl_2 (9:1) + 10^{-2} M NBu_4ClO_4, 298 K).

along the lanthanide series (Figure 5a).[26] Interestingly, the effective molarities, EM^{Ln}_{prox}, display the reverse order (Table 1, entry 7), which results in a compensation effect and the observation of intramolecular connection energies of similar magnitude along the series (Table 1, entries 8−10 and Figure 5b). Reasonably assuming similar entropic contributions to the effective molarities for Ln = La, Eu, and Lu,[27] the drastic decrease of EM^{Ln}_{prox} can assigned to increasing enthalpic constraints within the chelate rings induced by their coordination to smaller cations. This effect is strengthened by concomitant anticooperative interstrand and intermetallic interactions, which increase along the lanthanide series (Table 1, entries 11−16 and Figure 5c,d). The latter homocomponent interactions are responsible for the unusual selectivity of this ligand for the smaller lanthanides (Figure 5e).

Thermodynamic Predictions and Selective Detection of the Bimetallic [LaLu(L9)]$^{6+}$ Microspecies. In line with previous investigations,[9b,28] the thermodynamic constants collected in the Supporting Information, Table S5, for equilibria (eq 7) show a steeper electrostatic trend along the lanthanide series for the heterotopic N_2O site in **L11**, as compared with the N_3 binding unit in **L7**; an observation at the origin of the design of ligand **L10** for the selective complexation of large Ln(III) in the N_9 coordination site and small Ln(III) in the N_6O_3 coordination site in the C_3-symmetrical complexes *HHH*-$[Ln^1Ln^2(\mathbf{L10})_3]^{6+}$.[24,29] However, satisfying thermodynamic modeling and predictions failed because of the *HHH* ↔*HHT* isomerization processes operating in these binuclear helicates,[30] a limitation which is overcome in the non-isomerizable podates $[Ln^1Ln^2(\mathbf{L9})]^{6+}$. Equations 9−10 thus predict the stability of the two possible microspecies for the La/Lu pair (Supporting Information, Figure S6) where La(III) occupies either the proximal N_9 coordination site (eq 9, $[LaLu(\mathbf{L9})]^{6+}$ in Figure 6

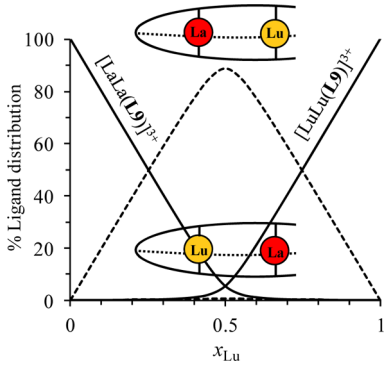

Figure 6. Predicted ($\Delta E_{mix} = 2\Delta E^{Lu,La} - (\Delta E^{La,La} + \Delta E^{Lu,Lu}) = 0$)[31] ligand distributions in the microspecies $[La_{2-x}Lu_x(\mathbf{L9})]^{6+}$ during the titration of $[La_2(\mathbf{L9})]^{6+}$ with $[Lu_2(\mathbf{L9})]^{6+}$ in absence of ligand dissociation (lutetium mole fractions $x_{Lu} = |Lu|_{tot}/(|La|_{tot} + |Lu|_{tot}) = 0-1$).

top) or the distal N_6O_3 coordination site (eq 10, $[LuLa(\mathbf{L9})]^{6+}$ in Figure 6 bottom).

$$\beta^{La,Lu,\mathbf{L9}}_{1,1,1} = 72(f^{La}_{N3})^3(f^{Lu}_{N2O})^3(EM^{La}_{prox})^2(EM^{Lu}_{prox})^2(0.69)^2 (u^{N3,N3}_{La})^3(u^{N2O,N2O}_{Lu})^3(u^{La,Lu}) \quad (9)$$

$$\beta^{Lu,La,\mathbf{L9}}_{1,1,1} = 72(f^{Lu}_{N3})^3(f^{La}_{N2O})^3(EM^{La}_{prox})^2(EM^{Lu}_{prox})^2(0.69)^2 (u^{N3,N3}_{Lu})^3(u^{N2O,N2O}_{La})^3(u^{Lu,La}) \quad (10)$$

All requested microscopic thermodynamic describers can be found in Table 1, except for the heterometallic interactions $u^{La,Lu}$ and $u^{Lu,La}$. Following the concept of the mixing rule depicted in eq 11,[31] and which has been experimentally justified for closely related bimetallic La/Lu helicates,[32] we calculate $u^{La,Lu} = u^{Lu,La} = e^{-(\Delta E^{Lu,La}/RT)} = (u^{La,La}u^{Lu,Lu})^{1/2} = 0.059$ for $[LaLu(\mathbf{L9})]^{6+}$ and $[LuLa(\mathbf{L9})]^{6+}$.

$$\Delta E^{La,Lu} = \Delta E^{Lu,La} = \frac{1}{2}(\Delta E^{La,La} + \Delta E^{Lu,Lu}) \quad (11)$$

Introducing the pertinent values of each describer into eqs 9 and 10 yields $\log(\beta^{La,Lu,\mathbf{L9}}_{1,1,1}) = 14.36$ and $\log(\beta^{Lu,La,\mathbf{L9}}_{1,1,1}) = 12.20$, from which the speciation in solution in absence of ligand dissociation can be foreseen (Figure 6).

The ratio of the microsconstants $\beta^{La,Lu,\mathbf{L9}}_{1,1,1}/\beta^{Lu,La,\mathbf{L9}}_{1,1,1} = 145$ indicates that the preferred microspecies with La(III) in the proximal site always counts for more than 99% of the ligand distribution in the heterometallic complexes, thus leading to high selectivity for the formation of a single bimetallic f-f′ microspecies. For a 10 mM total ligand concentration, the dissociation of $[Ln_2(\mathbf{L9})]^{6+}$ is negligible (Ln = La, Lu; Supporting Information, Figure S7) and the titration of $[La_2(\mathbf{L9})]^{6+}$ with $[Lu_2(\mathbf{L9})]^{6+}$ indeed leads to the formation of the bimetallic microspecies $[LaLu(\mathbf{L9})]^{6+}$ as the single novel complex, which is characterized by three ^1H NMR signals with identical intensities assigned to the diagnostic protons H5, H13, and H15 by using a combination of scalar (COSY) and dipolar (NOESY) H−H correlations (Figure 7).

The two extreme chemical shifts observed for H5 (low-field) and H13 (high-field) in $[LaLu(\mathbf{L9})]^{6+}$ (Figure 7b) are

dx.doi.org/10.1021/ic301631n | *Inorg. Chem.* 2012, 51, 10012−10024

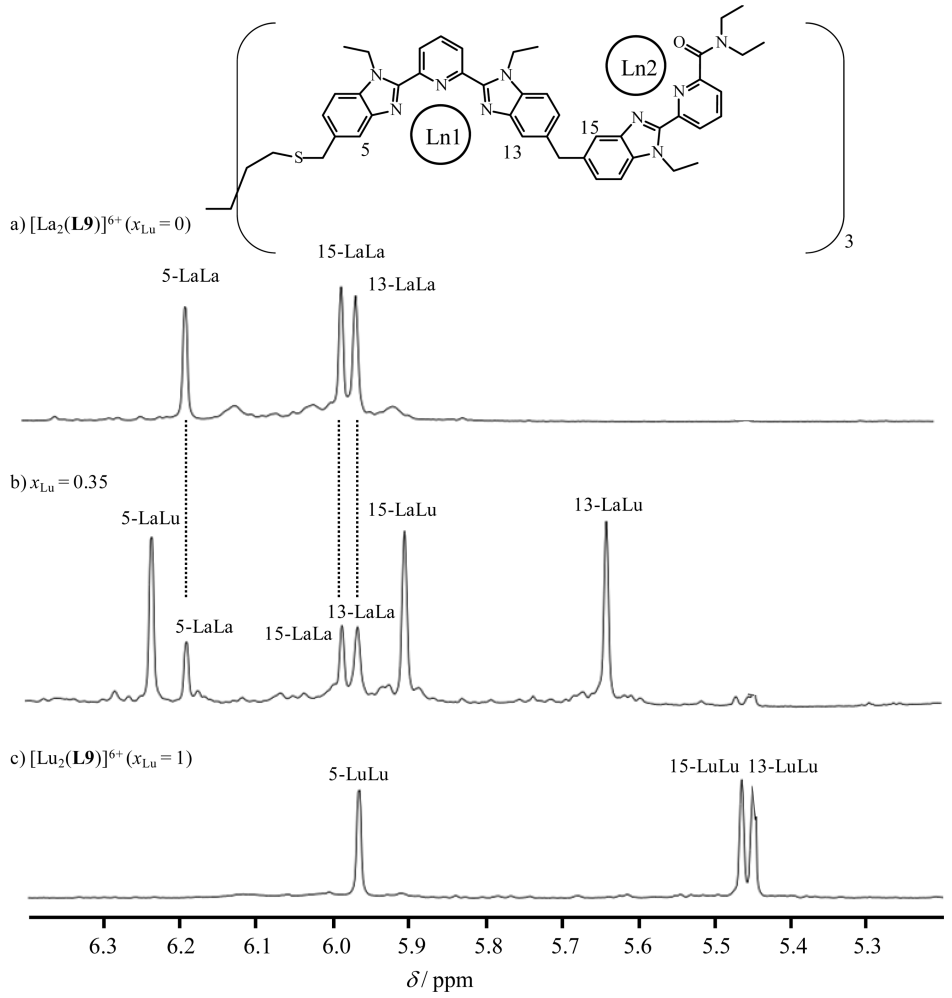

Figure 7. Aromatic parts of the ^{1}H NMR spectra showing the signals for the protons H5, H13, and H15 during the titration of $[La_2(\mathbf{L9})]^{6+}$ with $[Lu_2(\mathbf{L9})]^{6+}$ for (a) x_{Lu} = 0, (b) x_{Lu} = 0.35, and (c) x_{Lu} = 1.0 (CD_3CN, 298 K total ligand concentration 10 mM).

reminiscent from those observed in $[La_2(\mathbf{L9})]^{6+}$ (H5, Figure 7a) and in $[Lu_2(\mathbf{L9})]^{6+}$ (H13, Figure 7c), which rules out the alternative assignment to $[LuLa(\mathbf{L9})]^{6+}$. The same trend is systematically reproduced for the signals of the aromatic protons in $[LaLu(\mathbf{L9})]^{6+}$. The absence of significant signals for the alternative $[LuLa(\mathbf{L9})]^{6+}$ microspecies suggests that the application of the mixing rule for estimating $\Delta E^{La,Lu}$ is an acceptable approximation, as previously reported for related heterometallic f-f′ helicates.[32]

■ CONCLUSION

Whereas the successive metal loading of adjacent binding sites in single-stranded ligand is easily rationalized by using the classical Ising model with a unique intermetallic $\Delta E^{M,M}$ interaction,[18,31,33] the case of multistranded receptors possessing different binding sites and displaying mixed inter- and intramolecular connection processes remains essentially ignored.[34] To the best of our knowledge, this challenge has been only approached once with the thermodynamic study of triple-stranded helical ferric binders, in which two Fe(III) cations are bound to hydroxamic binding units incorporated into polyamide ribbons connected to a standard tris-aminoethylamine (TREN) tripod.[35] Depending on the length of the spacers separating the binding sites, some minor deviations from pure statistical binding could be detected,[35b] but the lack of explicit consideration of different Fe(III) affinity for each site (proximal and distal) prevents further exploitation of these results for thermodynamic programming and predictions. **L9** thus appears to be the first multistranded receptor, for which the various free energy contributions to the global complexation procceses have been deciphered (Figure 5). As expected, the driving force along the lanthanide series relies on the favorable contribution of the binding events (both inter- and intramolecular), but the selectivity depends on the interligand interactions, whereas the intermetallic interactions are marginal. Equipped with these microscopic describers, thermodynamic predictions are within the frame of reality, and the stability constants computed for the heterometallic $[LaLu(\mathbf{L9})]^{6+}$ and $[LuLa(\mathbf{L9})]^{6+}$ microspecies agree with preliminary solution speciations obtained by NMR titrations. According to Figure 8, the origin of the preference for the formation of $[LaLu(\mathbf{L9})]^{6+}$ with La(III) occupying the proximal site and Lu(III) lying in the distal site is spread over different factors, among which the specific microscopic affinity of each site for each metal is dominant. However, the physical roots of the successful application of the mixing rule for estimating the heterometallic interaction $\Delta E^{Ln1,Ln2}$ remain currently elusive since this parameter combines simple electrostatic repulsion with changes in solvation energies, both contributions being highly sensitive to the exact structure and shape of the complexes.[36] Further work will focus on the isolation of pure heterobimetallic lanthanide-

dx.doi.org/10.1021/ic301631n | Inorg. Chem. 2012, 51, 10012−10024

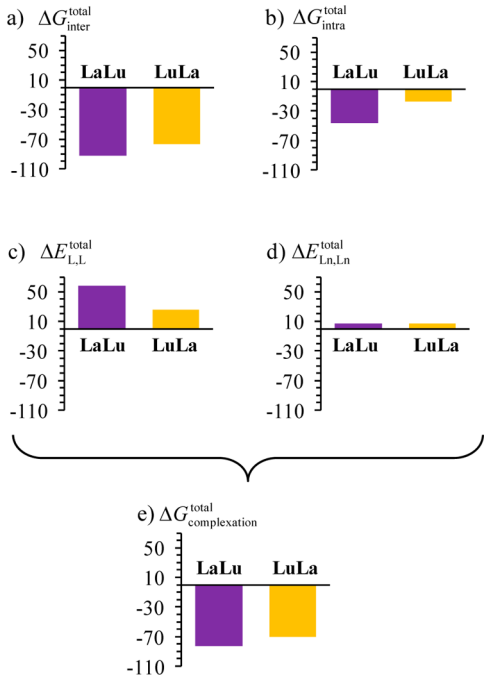

Figure 8. Representation of the thermodynamic contributions in kJ/mol corresponding to (a) intermolecular and (b) intramolecular Ln-ligand connections, and (c) interligand and (d) intermetallic interactions responsible for the global complexation process leading to $[LaLu(\mathbf{L9})]^{6+}$ (violet) and $[LuLa(\mathbf{L9})]^{6+}$ (orange) microspecies (CH_3CN/CH_2Cl_2 (9:1) + 10^{-2} M NBu_4ClO_4, 298 K).

containing podates displaying specific intermetallic communications for optical applications in molecular down- and upconversion processes.[37]

EXPERIMENTAL SECTION

Chemicals were purchased from Strem, Acros, Fluka AG, and Aldrich, and used without further purification unless otherwise stated. Ethyl-(4-methyl-2-nitro-phenyl)amine (**2**),[38] pyridine-2,6-dicarboxylic acid monomethyl ester (**4**),[39] 3,3′-dinitro-4,4′-bis(*N*-ethylamino)-diphenylmethane (**8**),[40] 1,5-dichloro-3-(2-chloro-ethyl)-3-methylpentane (**21**)[13] and the ligands **L7**,[41] **L8**,[11] **L11**,[28] and **L12**[10b] were prepared according to literature procedures. The trifluoromethanesulfonate salts $Ln(CF_3SO_3)_3{\cdot}xH_2O$ (Ln = La, Eu, Lu, x = 1−3) were prepared from the corresponding oxides (Aldrich, 99.99%).[42] The Ln content of solid salts was determined by complexometric titrations with Titriplex III (Merck) in the presence of urotropine and xylene orange.[43] Acetonitrile and dichloromethane were distilled over calcium hydride. Thin layer chromatography (TLC) used silicagel plates Merck 60 F_{254}, and Fluka silica gel 60 (0.04−0.063 mm) was used for preparative column chromatography.

Preparation of Methyl 6-(ethyl(4-(methoxymethyl)-2-nitrophenyl)carbamoyl)picolinate (5). Pyridine-2,6-dicarboxylic acid monomethyl ester (**4**, 6.48 g, 35.8 mmol) was refluxed for 1 h with thionyl chloride (25.0 mL, 358 mmol) and *N,N*′-dimethylformamide (0.01 mL) in dry dichloromethane (80 mL) under an inert atmosphere. After evaporation to dryness, the residual white solid was dried (10^{-2} Torr, 1 h), dissolved in dry dichloromethane (20 mL) and added dropwise to **2** (7.5 g, 35.8 mmol) in dichloromethane (20 mL) for 1 h. Diisopropylethylamine (6.1 mL, 35.8 mmol) in dichloromethane (20 mL) was then added, and the resulting mixture was refluxed for 2 h. The cooled organic phase was washed with half-sat. $NaHCO_3$ (2 × 100 mL) and half-sat. NH_4Cl (2 × 100 mL), dried over $MgSO_4$, filtered and evaporated to dryness. The crude residue was purified by column chromatography (silicagel, CH_2Cl_2:CH_3OH = 99:1) to give **5** as a yellow solid (5.5 g, 14.7 mmol, yield 41%). ^{1}H NMR ($CDCl_3$) δ/ppm: 8.12 (dd, ^3J = 7.8 Hz, ^4J = 1.2 Hz, 1H), 8.05 (dd, ^3J = 7.8 Hz, ^4J = 1.2 Hz, 1H), 7.98 (t, ^3J = 7.8 Hz, 2H), 7.81 (d, 1H, ^4J = 1.9 Hz), 7.54 (dd, ^3J = 8.1 Hz, ^4J = 1.9 Hz, 1H), 7.33 (d, ^3J = 8.1 Hz, 1H), 4.47 (s, 2H), 4.15 (dq, ^2J = 14.3 Hz, ^3J = 7.2 Hz, 1H), 3.94 (s, 3H), 3.72 (dq, ^2J = 14.3 Hz, ^3J = 7.2 Hz, 1H), 3.42 (s, 3H), 1.25 (t, ^3J = 7.2 Hz, 3H).

Preparation of 6-(Ethyl(4-(methoxymethyl)-2-nitrophenyl)-carbamoyl)picolinic acid (6). A solution of LiOH (3.1 g, 73.8 mmol) in water (35 mL) was dropwise added to a cooled (0 °C) solution of 6-(ethyl(4-(methoxymethyl)-2-nitrophenyl)carbamoyl)picolinate (**5**, 5.5 g, 14.7 mmol) in methanol (40 mL). The resulting mixture was stirred at 0 °C for 3 h, poured into water (600 mL) and washed with dichloromethane (4 × 100 mL). The aqueous phase was acidified at pH = 2 with conc. hydrochloric acid, and extracted with dichloromethane (4 × 100 mL). The combined organic phases were dried over Na_2SO_4, filtered and evaporated to dryness. The crude residue was purified by column chromatography (Silicagel, CH_2Cl_2:CH_3OH = 99:1) to give **6** as a pale yellow solid (4.5 g, 12.5 mmol, yield 88%). ^{1}H NMR ($CDCl_3$) δ/ppm: 8.16 (dd, ^3J = 7.8 Hz, ^4J = 1.2 Hz, 1H), 8.07 (dd, ^3J = 7.8 Hz, ^4J = 1.2 Hz, 1H), 7.97 (t, ^3J = 7.8 Hz, 2H), 7.83 (d, 1H, ^4J = 1.9 Hz), 7.56 (dd, ^3J = 8.1 Hz, ^4J = 1.9 Hz, 1H), 7.36 (d, ^3J = 8.1 Hz, 1H), 4.47 (s, 2H), 4.15 (dq, ^2J = 14.3 Hz, ^3J = 7.2 Hz, 1H), 3.79 (dq, ^2J = 14.3 Hz, ^3J = 7.2 Hz, 1H), 3.40 (s, 3H), 1.25 (t, ^3J = 7.2 Hz, 3H). ^{13}C NMR ($CDCl_3$) δ/ppm: 12.6, 46.8, 58.8, 72.5, 123.7, 125.1, 129.2, 131.0, 132.1, 135.4, 139.6, 140.9, 144.0, 146.9, 151.6, 163.3, 165.1.

Preparation of *N,N*-Diethyl-*N*-(4-(4-(ethylamino)-3-nitrobenzyl)-2-nitrophenyl)-*N*-(4-(methoxymethyl)-2-nitrophenyl)-pyridine-2,6-dicarboxamide (9). 6-(Ethyl(4-(methoxymethyl)-2-nitrophenyl)carbamoyl)picolinic acid (**6**, 1.13 g, 3.14 mmol) was refluxed for 1.5 h with thionyl chloride (2.5 mL, 31.4 mmol) and *N,N*′ dimethylformamide (0.01 mL) in dichloromethane (20 mL). After evaporation to dryness, the white residue was dried (10^{-2} Torr, 1 h), dissolved in dry dichloromethane (50 mL), and added dropwise to 3,3′-dinitro-4,4′-bis(*N*-ethylamino)diphenylmethane (**8**, 4.3 g, 12.6 mmol) in dichloromethane (100 mL) containing diisopropylethylamine (0.8 mL, 4.7 mmol). The resulting mixture was refluxed under an inert atmosphere for 12 h and evaporated to dryness. The orange solid was dissolved in dichloromethane (150 mL), washed successively with half-sat. NH_4Cl (180 mL), water (2 × 50 mL), and brine (50 mL). The organic phase was dried over Na_2SO_4, filtered and evaporated to dryness. The crude solid was purified by column chromatography (silicagel, CH_2Cl_2:CH_3OH = 100:0→99:1) to give **9** as an orange solid (1.59 g, 2.3 mmol, yield 74%). ESI-MS (CH_2Cl_2): m/z 686.3 ($[M+H]^+$), 708.6 ($[M+Na]^+$), 1372.8 ($[2M+H]^+$).

Preparation of 6-(*N,N*-Diethylcarbamoyl)pyridine-2-carboxylic acid (10). Pyridine-2,6-dicarboxylic acid monomethyl ester (**4**, 11.60 g, 64.0 mmol) was refluxed for 1 h with thionyl chloride (50.9 mL, 700 mmol) and *N,N*′-dimethylformamide (0.06 mL) in dichloromethane (100 mL). After evaporation to dryness, the white residue was dried (10^{-2} Torr, 1 h), dissolved in cooled dry dichloromethane (130 mL, 0 °C), and diethylamine (36.3 mL, 350 mmol) in dichloromethane (20 mL) was slowly added. The resulting mixture was refluxed for 2 h, then evaporated to dryness. The solid residue was partitioned between dichloromethane (250 mL) and brine (800 mL). The organic phase was separated, washed with water (250 mL), and evaporated to dryness. The resulting solid was dissolved in 1 M aq. sodium hydroxide (400 mL) and vigorously stirred for 10 min. The basic aqueous phase was washed with dichloromethane (2 × 100 mL), acidifed to reach pH = 2 with conc. hydrochloric acid, and the white precipitate was separated by filtration, dried, and recrystallized from hot acetonitrile to give **10** (12.88 g, 58 mmol, yield 91%). ^{1}H NMR ($CDCl_3$) δ/ppm: 8.27 (dd, ^3J = 7.8, ^4J = 0.9, 1H), 8.06 (t, ^3J = 7.8, 1H), 7.83 (dd, ^3J = 7.8, ^4J = 0.9, 1H), 3.59 (m, 2H), 3.30 (m, 2H), 1.29 (m, 3H), 1.21 (m, 3H).

Preparation of *N*-(4-(4-(6-(Diethylcarbamoyl)-*N*-ethylpicolinamido)-3-nitrobenzyl)-2-nitrophenyl)-*N,N*-diethyl-*N*-(4-(methoxymethyl)-2-nitrophenyl)pyridine-2,6-dicarboxamide (11). 6-(*N,N*-diethylcarbamoyl)pyridine-2-carboxylic acid (**10**, 2.2 g, 9.8 mmol) was refluxed for 1.5 h with thionyl chloride (2.9 mL, 40 mmol) and *N,N*′-dimethylformamide (0.01 mL) in dichloromethane (60 mL). After evaporation to dryness, the white residue was dried (10^{-2} Torr, 1 h), dissolved in dry dichloromethane (50 mL), and added to a dichloromethane solution (70 mL) containing **9** (2.7 g. 3.93 mmol) and

dx.doi.org/10.1021/ic301631n | *Inorg. Chem.* 2012, 51, 10012−10024

diisopropylethylamine (1.9 mL, 7.4 mmol). The resulting mixture was refluxed under an inert atmosphere for 12 h and evaporated to dryness. The residual solid was dissolved in dichloromethane (180 mL) and washed successively with half-sat. NH_4Cl (180 mL), water (50 mL), and brine (50 mL). The organic phase was dried over Na_2SO_4, filtered, and evaporated to dryness. The crude solid was purified by column chromatography (silicagel, CH_2Cl_2:CH_3OH = 100:0→98:2) to give **11** as a pale yellow solid (2.6 g, 3.1 mmol, 79%). ESI-MS ($CHCl_3$/MeOH): m/z 862.3 ($[M+H]^+$).

Preparation of *N*,*N*-Diethyl-6-(1-ethyl-5-((1-ethyl-2-(6-(1-ethyl-5-(methoxymethyl)-1*H*-benzo[d]imidazol-2-yl)pyridin-2-yl)-1*H*-benzo[d]imidazol-5-yl)methyl)-1*H*-benzo[d]imidazol-2-yl)picolinamide (12). *N*-(4-(4-(6-(diethylcarbamoyl)-*N*-ethylpicolinamido)-3-nitrobenzyl)-2-nitrophenyl)-*N*,*N*-diethyl-*N*-(4-(methoxymethyl)-2-nitrophenyl)pyridine-2,6-dicarboxamide (**9**, 1.77 g, 1.99 mmol) and activated metallic iron powder (2.77 g, 49.7 mmol) was refluxed in ethanol/water/conc. hydrochloric acid (200 mL/60 mL/12 mL) for 16 h. Excess of metallic iron was filtered off and ethanol was distilled under vacuum. Dichloromethane (150 mL) and Na_2H_2EDTA (19 g, 49.7 mmol in 250 mL water) was added to the remaining solution. The pH was adjusted to 7.0 with conc. aqueous ammonia. Conc. hydrogen peroxide (30% in water, 5 mL) was added dropwise under vigorous stirring, and the pH raised to 8.5 with conc. aqueous ammonia. The organic layer was separated, and the aqueous phase was extracted with dichloromethane (3 × 200 mL). The combined organic phases were washed with water (200 mL), dried over Na_2SO_4, filtered, and evaporated to dryness. The crude solid was purified by column chromatography (silicagel, CH_2Cl_2:CH_3OH = 100:0→97:3) to give **12** as a beige solid (1.2 g, 1.6 mmol, yield 81%). ^{1}H NMR ($CDCl_3$) δ/ppm: 8.37 (dd, ^3J = 8.0 Hz, ^4J = 1.0 Hz, 1H), 8.33 (dd, ^3J = 7.8 Hz, ^4J = 1.0 Hz, 1H), 8.32 (dd, ^3J = 7.9 Hz, ^4J = 1.1 Hz, 1H), 8.03 (t, ^3J = 7.9 Hz, 1H), 7.93 (t, ^3J = 7.8 Hz, 1H), 7.81 (d, ^4J = 1.0 Hz, 1H), 7.74 (d, ^4J = 1.0 Hz, 1H), 7.70 (d, ^4J = 1.0 Hz, 1H), 7.54 (dd, ^3J = 7.7 Hz, ^4J = 1.1 Hz), 7.46 (d, ^3J = 8.3 Hz, 1H), 7.35−7.39 (m, 3H), 7.24−7.27 (m, 2H), 4.72−4.82 (m, 6H), 4.62 (s, 2H), 4.30 (s, 2H), 3.61 (q, ^3J = 7.1 Hz, 2H), 3.41 (s, 3H), 3.35 (q, ^3J = 7.1 Hz, 2H), 1.45 (t, ^3J = 7.1 Hz, 3H), 1.35 (q, ^3J = 7.1 Hz, 6H), 1.28 (t, ^3J = 7.1 Hz, 3H), 1.07 (t, ^3J = 7.1 Hz, 3H). ^{13}C NMR ($CDCl_3$) δ/ppm: 12.8, 14.3, 15.3, 15.4, 39.5, 39.8, 39.9, 40.6, 42.2, 42.8, 57.8, 75.1, 110.0, 110.1, 110.2, 119.8, 120.0, 120.2, 122.4, 123.8, 124.9, 125.0, 125.5, 125.6, 132.9, 134.5, 134.8, 135.6, 136.5, 136.6, 137.9, 138.1, 142.9, 143.1, 143.3., 149.4, 149.5, 149.9, 150.1, 150.3, 154.5, 168.5. ESI-MS (CH_2Cl_2/MeOH 9:1): m/z 746.5 ($[M+H]^+$).

Preparation of 6-(1-Ethyl-5-{1-ethyl-2-[6-(1-ethyl-5-hydroxymethyl-1*H*-benzoimidazol-2-yl)-pyridin-2-yl]-1*H*-benzoimidazol-5-ylmethyl}-1*H*-benzoimidazol-2-yl)-pyridine-2-carboxylic Acid Diethylamide (13). A mixture of *N*,*N*-diethyl-6-(1-ethyl-5-((1-ethyl-2-(6-(1-ethyl-5-(methoxymethyl)-1*H*-benzo[d]imidazol-2-yl)-pyridin-2-yl)-1*H*-benzo[d]imidazol-5-yl)methyl)-1*H*-benzo[*d*]-imidazol-2-yl)picolinamide (**12**, 1.2 g, 1.6 mmol) in acetic anhydride/CH_2Cl_2 (25 mL/25 mL) and BF_3·Et_2O (1.0 mL, 8 mmol) was stirred for 16 h at room temperature, then poured into an ice-cooled aqueous 1 M KOH solution (400 mL). The aqueous layer was extracted with CH_2Cl_2 (2 × 50 mL). The combined organic phases were washed with deionized water until neutral, dried over Na_2SO_4, filtered, and evaporated to dryness to afford the crude acetate, which was dissolved in methanol/2 M aq. KOH (100 mL/70 mL), and stirred for 12 h at room temperature. The methanol was distilled under vacuum, the resulting solution was poured into brine (500 mL) and extracted with CH_2Cl_2 (3 × 100 mL). The combined organic phases were washed with deionized water until neutral, dried over Na_2SO_4, filtered, and evaporated to dryness. The resulting crude compound was purified by column chromatography (silicagel, CH_2Cl_2/MeOH 97:3 → 95:5) to afford **13** as a white solid (0.9 g, 1.2 mmol, yield 76%). ^{1}H NMR ($CDCl_3$) δ/ppm: 8.36 (dd, ^3J = 8.0 Hz, ^4J = 1.0 Hz, 1H), 8.23−8.27 (m, 2H), 7.95 (t, ^3J = 7.9 Hz, 1H), 7.92 (t, ^3J = 7.9 Hz, 1H), 7.77 (d, ^4J = 1.0 Hz, 1H), 7.74 (d, ^4J = 1.0 Hz, 1H), 7.69 (d, ^4J = 1.0 Hz, 1H), 7.53 (dd, ^3J = 7.7 Hz, ^4J = 1.0 Hz, 1H), 7.40−7.44 (m, 2H), 7.37 (d, ^3J = 8.4 Hz, 1H), 7.36 (d, ^3J = 8.4 Hz, 1H), 7.24 (dd, ^3J = 8.3 Hz, ^4J = 1.4 Hz, 2H), 4.82 (s, 2H), 4.71−4.79 (m, 6H), 4.29 (s, 2H), 3.60 (q, ^3J = 7.1 Hz, 2H), 3.35 (q, ^3J = 7.1 Hz, 2H), 1.45 (t, ^3J = 7.1 Hz, 3H), 1.26−1.37 (m, 9H), 1.07 (t, ^3J = 7.1 Hz, 3H). ^{13}C NMR ($CDCl_3$) δ/ppm: 12.8, 14.3, 15.4, 15.5, 39.6, 39.8, 39.9, 40.6, 42.2, 42.8, 65.6, 110.1, 110.2, 110.3, 118.8, 120.0, 120.1, 122.4, 123.3, 124.9, 125.0, 125.1, 125.5, 125.6, 134.5, 134.8, 135.5, 136.2, 136.6, 137.9, 142.9, 143.0, 143.1, 149.3, 149.4, 149.8, 149.9, 150.2, 154.4, 168.5. ESI-MS (CH_2Cl_2/MeOH 9:1): m/z 732.3 ($[M+H]^+$).

Preparation of 6-(5-{2-[6-(5-Chloromethyl-1-ethyl-1*H*-benzoimidazol-2-yl)-pyridin-2-yl]-1-ethyl-1*H*-benzoimidazol-5-ylmethyl}-1-ethyl-1*H*-benzoimidazol-2-yl)-pyridine-2-carboxylic Acid Diethylamide (14). A mixture of 6-(1-ethyl-5-{1-ethyl-2-[6-(1-ethyl-5-hydroxymethyl-1*H*-benzoimidazol-2-yl)-pyridin-2-yl]-1*H*-benzoimidazol-5-ylmethyl}-1*H*-benzoimidazol-2-yl)-pyridine-2-carboxylic acid diethylamide (**14**, 2.0 g, 2.7 mmol), CH_2Cl_2 (80 mL) and thionyl chloride (3.0 mL, 42 mmol) was stirred for 16 h at room temperature, then poured into aqueous sat. $NaHCO_3$ (650 mL). The aqueous layer was extracted with dichloromethane (3 × 100 mL), and the combined organic phases were washed with deionized water until neutral, dried over Na_2SO_4, filtered, and evaporated to dryness. The resulting crude compound was purified by column chromatography (silicagel, CH_2Cl_2/MeOH 98:2 → 95:5) to afford **14** as a beige solid (1.95 g, 2.6 mmol, yield 99%). ^{1}H NMR ($CDCl_3$) δ/ppm: 8.39 (d, ^3J = 7.9 Hz, 1H), 8.30−8.35 (m, 2H), 8.04 (t, ^3J = 7.8 Hz, 1H), 7.93 (t, ^3J = 7.8 Hz, 1H), 7.86 (d, ^4J = 1.0 Hz, 1H), 7.74 (d, ^4J = 1.0 Hz, 1H), 7.71 (s, 1H), 7.54 (dd, ^3J = 7.8 Hz, ^4J = 1.0 Hz, 1H), 7.43 (dd, ^3J = 8.3 Hz, ^4J = 0.5 Hz, 1H), 7.42 (dd, ^3J = 8.3 Hz, ^4J = 1.5 Hz, 1H), 7.38 (d, ^3J = 8.3 Hz, 1H), 7.37 (d, ^3J = 8.3 Hz, 1H), 7.27 (t, ^4J = 1.0 Hz, 1H), 7.25 (t, ^4J = 1.0 Hz, 1H), 4.79 (s, 2H), 4.71−4.78 (m, 6H), 4.30 (s, 2H), 3.61 (q, ^3J = 7.1 Hz, 2H), 3.35 (q, ^3J = 7.1 Hz, 2H), 1.45 (t, ^3J = 7.1 Hz, 3H), 1.32−1.38 (m, 6H), 1.29 (t, ^3J = 7.1 Hz, 3H), 1.07 (t, ^3J = 7.1 Hz, 3H). ^{13}C NMR ($CDCl_3$) δ/ppm: 12.8, 14.3, 15.3, 15.4, 39.5, 39.8, 39.9, 40.6, 42.2, 42.8, 47.2, 110.1, 110.2, 110.7, 120.0, 120.2, 120.6, 122.5, 124.5, 125.0, 125.7, 125.8, 132.3, 134.5, 134.8, 136.0, 136.7, 138.0, 138.2, 142.9, 143.1, 149.3, 149.7, 149.8, 150.1, 150.8, 154.5, 168.5; ESI-MS (CH_2Cl_2/MeOH 9:1): m/z 750.3 ($[M+H]^+$).

Preparation of Thioacetic acid S-[2-(6-{5-[2-(6-diethylcarbamoyl-pyridin-2-yl)-1-ethyl-1*H*-benzoimidazol-5-ylmethyl]-1-ethyl-1*H*-benzoimidazol-2-yl}-pyridin-2-yl)-1-ethyl-1*H*-benzoimidazol-5-ylmethyl] Ester (15). 6-(5-{2-[6-(5-Chloromethyl-1-ethyl-1*H*-benzoimidazol-2-yl)-pyridin-2-yl]-1-ethyl-1*H*-benzoimidazol-5-ylmethyl}-1-ethyl-1*H*-benzoimidazol-2-yl)-pyridine-2-carboxylic acid diethylamide (**14**, 2.0 g, 2.6 mmol) was dissolved in a suspension of potassium thioacetate (1.5 g, 13.3 mmol) in acetone (40 mL) and dichloromethane (40 mL). The mixture was refluxed for 16 h, and then evaporated to dryness. The resulting solid was partitioned between dichloromethane (400 mL) and water (300 mL). The aqueous phase was separated and extracted with dichloromethane (3 × 100 mL). The combined organic phases were washed with brine, dried over Na_2SO_4, filtered, evaporated, and the residue was purified by column chromatography (silicagel, CH_2Cl_2/MeOH 100:0 → 95:5) to afford **15** as a white solid (2.0 g, 2.5 mmol, yield 96%). ^{1}H NMR ($CDCl_3$) δ/ppm: 8.37 (dd, ^3J = 8.0 Hz, ^4J = 1.0 Hz, 1H), 8.32 (dd, ^3J = 7.8 Hz, ^4J = 1.0 Hz, 1H), 8.30 (dd, ^3J = 7.8 Hz, ^4J = 1.0 Hz, 1H), 8.02 (t, ^3J = 7.8 Hz, 1H), 7.92 (t, ^3J = 7.8 Hz, 1H), 7.77 (d, ^4J = 1.0 Hz, 1H), 7.73 (d, ^4J = 1.0 Hz, 1H), 7.70 (d, ^4J = 1.0 Hz, 1H), 7.53 (dd, ^3J = 7.7 Hz, ^4J = 1.0 Hz, 1H), 7.35−7.40 (m, 3H), 7.30 (dd, ^3J = 8.4 Hz, ^4J = 1.5 Hz, 1H), 7.26 (m, 1H), 7.24 (t, ^4J = 1.5 Hz, 1H), 4.71−4.78 (m, 6H), 4.30 (s, 4H), 3.60 (q, ^3J = 7.1 Hz, 3H), 3.35 (q, ^3J = 7.1 Hz, 2H), 2.35 (s, 3H), 1.45 (t, ^3J = 7.1 Hz, 3H), 1.30−1.35 (m, 6H), 1.28 (t, ^3J = 7.1 Hz, 3H), 1.07 (t, ^3J = 7.1 Hz, 3H). ^{13}C NMR ($CDCl_3$) δ/ppm: 12.8, 14.3, 15.3, 15.4, 15.5, 30.4, 34.0, 39.6, 39.8, 39.9, 40.6, 42.2, 42.8, 110.0, 110.2, 110.4, 120.0, 120.2, 120.4, 122.4, 124.6, 124.9, 125.0, 125.1, 125.6, 125.7, 132.3, 134.5, 134.8, 135.3, 136.5, 136.6, 137.9, 138.0, 143.0, 143.1, 143.2, 149.3, 149.4, 149.8, 149.9, 150.1, 150.5, 154.4, 168.5, 195.2. ESI-MS (CH_2Cl_2/MeOH 9:1): m/z 790.3 ($[M+H]^+$).

Preparation of 6-(1-Ethyl-5-{1-ethyl-2-[6-(1-ethyl-5-mercaptomethyl-1*H*-benzoimidazol-2-yl)-pyridin-2-yl]-1*H*-benzoimidazol-5-ylmethyl}-1*H*-benzoimidazol-2-yl)-pyridine-2-carboxylic Acid Diethylamide (16). Thioacetic acid S-[2-(6-{5-[2-(6-diethylcarbamoyl-pyridin-2-yl)-1-ethyl-1*H*-benzoimidazol-5-ylmethyl]-1-ethyl-1*H*-benzoimidazol-2-yl}-pyridin-2-yl)-1-ethyl-1*H*-benzoimidazol-5-ylmethyl] ester (**15**, 1.1 g, 1.4 mmol) was dissolved in degassed methanol (60 mL) containing conc. hydrochloric acid (37%, 5 mL). The

dx.doi.org/10.1021/ic301631n | *Inorg. Chem.* 2012, 51, 10012−10024

mixture was stirred and heated at 45 °C for 16 h under an inert atmosphere. The methanol was then evaporated, and the solid residue was partitioned between ethyl acetate (450 mL) and water (600 mL) containing $NaHCO_3$ (10.4 g, 123 mmol). The aqueous phase was separated and extracted with ethyl acetate (3 × 100 mL). The combined organic phases were washed with brine, dried over Na_2SO_4, filtered, and evaporated to yield a pale yellow solid, which was purified by column chromatography (silicagel, CH_2Cl_2/MeOH 98:2 → 95:5) to afford **16** as a white solid (0.88 g, 1.2 mmol, 81%). ^{1}H NMR ($CDCl_3$) δ/ppm: 8.38 (dd, ^3J = 8.0 Hz, ^4J = 0.9 Hz, 1H), 8.32 (dd, ^3J = 7.8 Hz, ^4J = 1.0 Hz, 1H), 8.31 (dd, ^3J = 7.9 Hz, ^4J = 1.0 Hz, 1H), 8.02 (t, ^3J = 7.9 Hz, 1H), 7.92 (t, ^3J = 7.9 Hz, 1H), 7.77 (d, ^4J = 0.8 Hz, 1H), 7.73 (d, ^4J = 0.5 Hz, 1H), 7.70 (d, ^4J = 0.5 Hz, 1H), 7.53 (dd, ^3J = 7.7 Hz, ^4J = 1.0 Hz, 1H), 7.42 (d, ^3J = 8.4 Hz, 1H), 7.34−7.38 (m, 3H), 7.24−7.27 (m, 2H), 4.71−4.80 (m, 6H), 4.30 (s, 2H), 3.91 (d, ^3J = 7.4 Hz, 2H), 3.60 (q, ^3J = 7.1 Hz, 2H), 3.35 (q, ^3J = 7.1 Hz, 2H), 1.83 (t, ^3J = 7.4 Hz, 1H), 1.45 (t, ^3J = 7.1 Hz, 3H), 1.25−1.36 (m, 9H), 1.07 (t, ^3J = 7.1 Hz, 3H). ^{13}C NMR ($CDCl_3$) δ/ppm: 12.8, 14.1, 14.3, 15.4, 15.5, 29.4, 39.5, 39.8, 39.9, 40.6, 42.2, 42.8, 110.0, 110.2, 110.5, 119.4, 120.0, 120.2, 122.4, 124.1, 124.9, 125.0, 125.1, 125.6, 125.7, 134.5, 134.8, 135.1, 136.1, 136.5, 136.6, 137.9, 138.1, 142.9, 143.0, 143.2., 149.3, 149.4, 149.8, 150.1, 150.4, 154.5, 168.5. ESI-MS (CH_2Cl_2/MeOH 9:1): m/z 748.5 ($[M+H]^+$).

Preparation of Ligand L9. All reactants and solvents were carefully dried and degassed prior to be used. 6-(1-Ethyl-5-{1-ethyl-2-[6-(1-ethyl-5-mercaptomethyl-1*H*-benzoimidazol-2-yl)-pyridin-2-yl]-1*H*-benzoimidazol-5-ylmethyl}-1*H*-benzoimidazol-2-yl)-pyridine-2-carboxylic acid diethylamide (**16**, 1.39 g, 1.86 mmol) and 1,5-dichloro-3-(2-chloroethyl)-3-methyl-pentane (**21**, 0.114 g, 0.53 mmol) were dissolved in a suspension of cesium carbonate (0.61 g, 1.86 mmol) in freshly distilled DMF (20 mL) under a nitrogen atmosphere. The mixture was stirred, heated at 60 °C for 16 h, filtered, and evaporated to dryness. The resulting solid was dissolved in dichloromethane (100 mL) and water (100 mL). The organic phase was washed with water (50 mL) and brine (50 mL), dried over Na_2SO_4, filtered, and evaporated to dryness to yield a solid residue, which was purified by column chromatography (silicagel, CH_2Cl_2/MeOH 98:2 → 92:8) to afford **L9** as a pale yellow solid (0.65 g, 0.28 mmol, yield 53%). ^{1}H NMR ($CDCl_3$) δ/ppm: 8.37 (d, ^3J = 7.8 Hz, 3H), 8.29 (d, ^3J = 7.9 Hz, 6H), 7.97 (t, ^3J = 7.9 Hz, 3H), 7.91 (t, ^3J = 7.8 Hz, 3H), 7.72 (s, 6H), 7.69 (s, 3H), 7.53 (d, ^3J = 7.8 Hz, 3H), 7.34−7.38 (m, 9H), 7.29 (dd, ^3J = 8.4 Hz, ^4J = 1.0 Hz, 3H), 7.22−7.26 (m, 6H), 4.71−4.74 (m, 18H), 4.28 (s, 6H), 3.80 (s, 6H), 3.60 (q, ^3J = 7.1 Hz, 6H), 3.34 (q, ^3J = 7.1 Hz, 6H), 2.25−2.28 (m, 6H), 1.37−1.45 (m, 15H), 1.24−1.34 (m, 27H), 1.06 (t, ^3J = 7.1 Hz, 9H), 0.75 (s, 3H). ^{13}C NMR ($CDCl_3$) δ/ppm: 12.9, 14.4, 15.4, 15.5, 24.4, 26.0, 29.8, 36.6, 36.8, 39.0, 39.7, 39.9, 40.0, 40.7, 42.3, 42.9, 110.1, 110.3, 110.5, 115.7, 120.0, 120.2, 120.3, 122.5, 124.8, 125.0, 125.1, 125.4, 125.7, 125.7, 125.9, 133.1, 134.6, 134.9, 135.2, 136.7, 138.0, 138.1, 138.3, 143.0, 143.2, 149.3, 149.4, 149.9, 150.0, 150.3, 154.5, 168.6. ESI-MS (CH_2Cl_2/MeOH 9:1): m/z 2352.9 ($[M+H]^+$), 1176.8 ($[M+2H]^{2+}$). Elemental analyses: calcd for $C_{140}H_{147}N_{27}O_3S_3{\cdot}4H_2O$ %C 69.36, %H 6.44, %N 15.60. Found %C 69.21, %H 6.19, %N 15.43.

Preparation of the Complexes $[La_2(L9)](CF_3SO_3)_6{\cdot}16H_2O$ and $[Lu_2(L9)](CF_3SO_3)_6{\cdot}12H_2O$. A solution of $Ln(CF_3SO_3)_3{\cdot}xH_2O$ (Ln = La or Lu, 21 μmol) in acetonitrile (4 mL) was added to a solution of **L9**·4H_2O (25.5 mg, 10.5 μmol) in dichloromethane (4 mL). The resulting pale yellow mixture was stirred for 12 h, then evaporated to dryness. The residue was dissolved in acetonitrile and diethyl ether was slowly added to precipitate the complex. The resulting pale yellow microcrystalline powders were collected by fitration and dried to give $[Ln_2(L9)](CF_3SO_3)_6{\cdot}xH_2O$ (Ln = La, x = 16; Ln = Lu, x = 12).

$[La_2(L9)](CF_3SO_3)_6{\cdot}16H_2O$. (yield 67%). ^{1}H NMR (CD_3CN) δ/ppm: 8.30 (m, 6H), 8.11 (t, ^3J = 8.1 Hz, 3H), 7.92 (d, ^3J = 8.1 Hz, 3H), 7.70−7.75 (m, 6H), 7.64 (m, 6H), 7.37 (dd, ^3J = 8.5 Hz, ^4J = 0.8 Hz, 3H), 7.30 (dd, ^3J = 8.7 Hz, ^4J = 1.0 Hz, 3H), 7.19 (d, ^3J = 8.3 Hz, 3H), 7.02 (dd, ^3J = 8.3 Hz, ^4J = 0.7 Hz, 3H), 6.18 (s, 3H), 5.98 (s, 3H), 5.96 (s, 3H), 4.69 (sext., ^2J = 15.1 Hz, ^3J = 7.2 Hz, 3H), 4.39−4.51 (m, 9H), 4.31 (sext., ^2J = 15.1 Hz, ^3J = 7.2 Hz, 3H), 4.18 (sext., ^2J = 15.0 Hz, ^3J = 7.2 Hz, 3H), 3.71 (d, ^2J = 17.9 Hz, 3H), 3.54 (d, ^2J = 17.9 Hz, 3H), 3.44 (d, ^2J = 14.8 Hz, 3H), 3.35 (sext., ^2J = 14.7 Hz, ^3J = 7.1 Hz, 3H), 3.24 (sext., ^2J = 14.7 Hz, ^3J = 7.1 Hz, 3H), 2.81 (sext., ^2J = 13.3 Hz, ^3J = 7.1 Hz, 3H), 2.74 (d, ^2J = 14.8 Hz, 3H), 2.68−2.77 (m, 3H), 1.49−1.53 (m, 18H), 1.21−1.30 (m, 3H), 1.23 (t, ^3J = 7.2 Hz, 9H), 0.82−0.88 (m, 3H), 0.78 (t, ^3J = 7.1 Hz, 9H), 0.71 (t, ^3J = 7.1 Hz, 9H), 0.32 (s, 3H), 0.13−0.26 (m, 6H). ^{13}C NMR (CD_3CN) δ/ppm: 11.3, 12.9, 14.3, 14.7, 23.1, 29.4, 34.0, 35.6, 38.2, 39.2, 41.5, 41.9, 42.0, 42.7, 45.0, 111.3, 111.9, 112.6, 116.1, 119.6, 122.8, 124.8, 125.7, 126.0, 126.5, 126.9, 127.1, 127.5, 127.8, 133.1, 133.6, 134.3, 136.0, 136.1, 138.5, 139.6, 139.8, 142.6, 143.5, 145.6, 146.4, 147.0, 149.5, 149.6, 149.8, 151.1, 168.8. Elemental analyses: calcd for $La_2C_{146}H_{147}N_{27}O_{21}S_9F_{18}{\cdot}16H_2O$ (MM = 3812.54) %C 45.99, %H 4.73, %N 9.92. Found %C 45.87, %H 4.29, %N 9.80.

$[Lu_2(L9)](CF_3SO_3)_6{\cdot}12H_2O$ (yield 41%). ^{1}H NMR (CD_3CN) δ/ppm: 8.38 (d, ^3J = 8.2 Hz, 3H), 8.25 (t, ^3J = 8.1 Hz, 3H), 7.92 (t, ^3J = 8.1 Hz, 3H), 7.73 (dd, ^3J = 8.0 Hz, 6H), 7.65 (dd, ^3J = 8.6 Hz, 6H), 7.59 (d, ^3J = 8.2 Hz, 3H), 7.31 (dd, ^3J = 8.6 Hz, ^4J = 1.6 Hz, 6H), 7.25 (d, ^3J = 8.3 Hz, 3H), 7.94 (dd, ^3J = 8.4 Hz, ^4J = 1.5 Hz, 3H), 5.97 (d, ^4J = 1.4 Hz, 3H), 5.46 (s, 3H), 5.44 (s, 3H), 4.78 (dq, ^2J = 14.0 Hz, ^3J = 6.8 Hz, 3H), 4.61 (dq, ^2J = 14.6 Hz, ^3J = 7.3 Hz, 3H), 4.52 (tt, ^2J = 14.5 Hz, ^3J = 7.3 Hz, 6H), 4.36 (dq, ^2J = 14.6 Hz, ^3J = 7.2 Hz, 3H), 4.28 (dt, ^2J = 14.8 Hz, ^3J = 7.4 Hz, 3H), 3.62 (d, ^2J = 17.4 Hz, 3H), 3.50 (d, ^2J = 17.4 Hz, 3H), 3.40−3.27 (m, 6H), 2.75−2.63 (m, 6H), 2.62−2.52 (m, 3H), 1.52−1.44 (m, 24H), 1.42−1.22 (m, 3H), 1.04 (t, ^3J = 7.1 Hz, 3H), 0.90 (td, ^2J = 12.7 Hz, ^3J = 5.8 Hz, 3H), 0.62 (t, ^3J = 7.1 Hz, 9H), 0.36 (s, 3H), 0.25 (m, 6H). Elemental analyses: calcd for $Lu_2C_{146}H_{147}N_{27}O_{21}S_9F_{18}{\cdot}12H_2O$ (MM = 3812.60) %C 45.8, %H 4.52, %N 9.92. Found %C 45.95, %H 4.26, %N 9.91.

Spectroscopic Measurements. Electronic spectra in the UV−vis were recorded at 20 °C from solutions in CH_3CN with a Perkin-Elmer Lambda 900 spectrometer using quartz cells of 0.1 or 1 mm path length. Spectrophotometric titrations were performed with a J&M diode array spectrometer (Tidas series) connected to an external computer. In a typical experiment, 25 mL of **L9** (10^{-4} M) in CH_3CN/CH_2Cl_2 (9:1) + 10^{-2} M NBu_4ClO_4 were titrated at 25 °C with a solution of $Ln(CF_3SO_3)_3{\cdot}xH^2O$ (10^{-3} M) in the same solvent under an inert atmosphere. After each addition of 0.10 mL, the absorbance was recorded using Hellma optrodes (optical path length 0.1 cm) immersed in the thermostatted titration vessel and connected to the spectrometer. Mathematical treatment of the spectrophotometric data was performed with factor analysis[43] and with the SPECFIT program.[17] ^{1}H and ^{13}C NMR spectra were recorded at 25 °C on a Bruker Avance 400 MHz and Bruker DRX-500 MHz spectrometers. Chemical shifts are given in ppm with respect to TMS. Pneumatically assisted electrospray (ESI-MS) mass spectra were recorded from 10^{-4} M solutions on a Finnigan SSQ7000 instrument or on an Applied Biosystems API 150EX LC/MS System equipped with a Turbo Ionspray source. Elemental analyses were performed by K. L. Buchwalder from the Microchemical Laboratory of the University of Geneva. Least-squares fitting methods were implemented in Excel and Mathematica.

■ ASSOCIATED CONTENT

Ⓢ Supporting Information

Tables of ^{1}H NMR chemical shifts, ESI-MS titrations, and thermodynamic stability constants. Figures illustrating the application of the site binding model, correlation between calculated and experimental thermodynamic stability constants and ligand distributions. This material is available free of charge via the Internet at http://pubs.acs.org.

■ AUTHOR INFORMATION

Corresponding Author

*E-mail: Gabriel.Canard@univ-amu.fr (G.C.), Claude.Piguet@unige.ch (C.P.).

Notes

The authors declare no competing financial interest.

■ ACKNOWLEDGMENTS

Financial support from the Swiss National Science Foundation is gratefully acknowledged.

REFERENCES

(1) (a) Hancock, R. D. *J. Chem. Educ.* **1992**, *69*, 615−621. (b) Motekaitis, R. J.; Martell, A. E.; Hancock, R. D. *Coord. Chem. Rev.* **1994**, *133*, 39−65.

(2) (a) Constable, E. C. *Adv. Inorg. Chem.* **1989**, *34*, 1−63. (b) Keene, F. R. *Dalton Trans.* **2011**, *40*, 2405−2418.

(3) Amendola, V.; Fabbrizzi, L.; Mangano, C.; Lanfredi, A. M.; Pallavicini, P.; Perotti, F.; Ugozzoli, F. *J. Chem.. Soc., Dalton Trans.* **2000**, 1155−1160.

(4) Krenske, E.; Gahan, L. R. *Aust. J. Chem.* **2002**, *55*, 761−766.

(5) (a) Lutz, A.; Ward, T. R.; Albrecht, M. *Tetrahedron* **1996**, *52*, 12197−12208. (b) Ward, T. R.; Lutz, A.; Parel, S. P.; Ensling, J.; Gütlich, P.; Buglyo, P.; Orvig, C. *Inorg. Chem.* **1999**, *38*, 5007−5017.

(6) (a) Chapman, R. D.; Loda, R. T.; Riehl, J. P.; Schwartz, R. W. *Inorg. Chem.* **1984**, *23*, 1652−1657. (b) Constable, E. C. *Adv. Inorg. Chem. Radiochem.* **1986**, *30*, 69−121. (c) Kepert, C. J.; Lu, W.-M.; Semenova, L. J.; Skelton, B. W.; White, A. H. *Aust. J. Chem.* **1999**, *52*, 481−496.

(7) Bretonnière, Y.; Mazzanti, M.; Wietzke, R.; Pécaut, J. *Chem. Commun.* **2000**, 1543−1544 . Please note that the use of amide connectors in **L6** lead to a total number of 12 potential binding sites (9N and 3O donors), which contributed to the obervation of a complicate mixture of $[Ln(\mathbf{L6})]^{3+}$, $[Ln_3(\mathbf{L6})_2]^{9+}$ (major species), and $[Ln_2(\mathbf{L6})]^{6+}$ complexes in solution in intermediate exchange on the NMR timescale, whereas only $[Ln_3(\mathbf{L6})_2(CF_3SO_3)_4(H_2O)_2](CF_3SO_3)_5$ could be characterized in the solid state.

(8) Piguet, C.; Bünzli, J.-C. G.; Bernardinelli, G.; Williams, A. F. *Inorg. Chem.* **1993**, *32*, 4139−4149.

(9) (a) Piguet, C.; Bünzli, J.-C. G.; Bernardinelli, G.; Bochet, C. G.; Froidevaux, P. *J. Chem. Soc., Dalton Trans.* **1995**, 83−97. (b) Petoud, S.; Bünzli, J.-C. G.; Renaud, F.; Piguet, C.; Schenk, K. J.; Hopfgartner, G. *Inorg. Chem.* **1997**, *36*, 5750−5760.

(10) (a) Koeller, S.; Bernardinelli, G.; Bocquet, B.; Piguet, C. *Chem.—Eur. J.* **2003**, *9*, 1062−1074. (b) Koeller, S.; Bernardinelli, G.; Piguet, C. *Dalton Trans.* **2003**, 2395−2404. (c) Koeller, S.; Bernardinelli, G.; Piguet, C. *C. R. Chim.* **2006**, *9*, 1158−1162.

(11) Canard, G.; Koeller, S.; Bernardinelli, G.; Piguet, C. *J. Am. Chem. Soc.* **2008**, *130*, 1025−1040.

(12) (a) Costes, J.-P.; Dahan, F.; Dupuis, A.; Lagrave, S.; Laurent, J.-P. *Inorg. Chem.* **1998**, *37*, 153−155. (b) Brianese, N.; Casellato, U.; Tamburini, S.; Tomasin, P.; Vigato, P. A. *Inorg. Chim. Acta* **1998**, *272*, 235−251. (c) Bretonnière, Y.; Wietzke, R.; Lebrun, C.; Mazzanti, M.; Pécaut, J. *Inorg. Chem.* **2000**, *39*, 3499−3505. (d) Charbonnière, L. J.; Ziessel, R.; Guardigli, M.; Roda, A.; Sabbatini, N.; Cesario, M. *J. Am. Chem. Soc.* **2001**, *123*, 2436−2437. (e) Costes, J.-P.; Nicodème, F. *Chem.—Eur. J.* **2002**, *8*, 3442−3447. (f) Bismondo, A.; Di Bernardo, P.; Portanova, R.; Tolazzi, M.; Zanonato, P. L. *Polyhedron* **2002**, *21*, 1393−1396. (g) Costes, J.-P.; Dahan, F.; Nicodème, F. *Inorg. Chem.* **2003**, *42*, 6556−6563. (h) Comby, S.; Imbert, D.; Vandevyver, C.; Bünzli, J.-C. G. *Chem.—Eur. J.* **2007**, *13*, 936−944. (i) Chandrasekhar, V.; Pandian, B. M.; Azhakar, R.; Vittal, J. J.; Clérac, R. *Inorg. Chem.* **2007**, *46*, 5140−5142. (j) Nonat, A.; Imbert, D.; Pécaut, J.; Giraud, M.; Mazzanti, M. *Inorg. Chem.* **2009**, *48*, 4207−4218. (k) Moore, E. G.; Samuel, A. P. S.; Raymond, K. N. *Acc. Chem. Res.* **2009**, *42*, 542−552 , and references therein.

(13) Baumeister, J. M.; Alberto, R.; Ortner, K.; Spingler, B.; August Schubiger, P.; Kaden, T. A. *J. Chem. Soc., Dalton Trans.* **2002**, 4143−4151.

(14) (a) Piguet, C.; Rivara-Minten, E.; Hopfgartner, G.; Bünzli, J.-C. G. *Helv. Chim. Acta* **1995**, *78*, 1541−1566. (b) Piguet, C.; Bünzli, J.-C. G.; Bernardinelli, G.; Hopfgartner, G.; Petoud, S.; Schaad, O. *J. Am. Chem. Soc.* **1996**, *118*, 6681−6697.

(15) Nakamoto, K. *J. Phys. Chem.* **1960**, *64*, 1420−1425.

(16) Dalla Favera, N.; Hamacek, J.; Borkovec, M.; Jeannerat, D.; Gumy, F.; Bünzli, J.-C. G.; Ercolani, G.; Piguet, C. *Chem.—Eur. J.* **2008**, *14*, 2994−3005.

(17) (a) Gampp, H.; Maeder, M.; Meyer, C. J.; Zuberbühler, A. *Talanta* **1985**, *32*, 1133−1139. (b) Gampp, H.; Maeder, M.; Meyer, C. J.; Zuberbühler, A. *Talanta* **1986**, *33*, 943−951.

(18) (a) Hamacek, J.; Borkovec, M.; Piguet, C. *Dalton Trans.* **2006**, 1473−1490. (b) Piguet, C. *Chem. Commun.* **2010**, *46*, 6209−6231.

(19) (a) Schwarzenbach, G. *Helv. Chim. Acta* **1952**, *35*, 39−65. (b) Adamson, A. W. *J. Am. Chem. Soc.* **1954**, *76*, 1578−1579. (c) Martell, A. E. *Adv. Chem. Ser.* **1966**, *62*, 272−294. (d) Munro, D. *Chem. Brit.* **1977**, *13*, 100−105. (e) Simmons, E. L. *J. Chem. Educ.* **1979**, *56*, 578−579. (f) Chung, C.-S. *J. Chem. Educ.* **1984**, *61*, 1062−1064.

(20) (a) Benson, S. W. *J. Am. Chem. Soc.* **1958**, *80*, 5151−5154. (b) Bailey, W. F.; Monahan, A. S. *J. Chem. Educ.* **1978**, *55*, 489−493. (c) Ercolani, G.; Piguet, C.; Borkovec, M.; Hamacek, J. *J. Phys. Chem. B* **2007**, *111*, 12195−12203.

(21) For simplification purpose, each tridentate binding unit is considered as a single point connector for the entering metal.

(22) (a) Ercolani, G.; Mandolini, L.; Mencarelli, P.; Roelens, S. *J. Am. Chem. Soc.* **1993**, *115*, 3901−3908. (b) Kitov, P. I.; Bundle, D. R. *J. Am. Chem. Soc.* **2003**, *125*, 16271−16284. (c) Mulder, A.; Huskens, J.; Reinhoudt, D. N. *Org. Biomol. Chem.* **2004**, *2*, 3409−3424. (d) Williams, D. H.; Stephens, E.; O'Brien, D. P.; Zhou, M. *Angew. Chem., Int. Ed.* **2004**, *43*, 6596−6616. (e) Badjic, J. D.; Nelson, A.; Cantrill, S. J.; Turnbull, W. B.; Stoddart, J. F. *Acc. Chem. Res.* **2005**, *38*, 723−732. (f) Schneider, H.-J.; Yatsimirsky, A. K. *Chem. Soc. Rev.* **2008**, *37*, 263−277. (g) Rehm, T.; Schmuck, C. *Chem. Commun.* **2008**, 801−813.

(23) (a) Kuhn, W. *Kolloid Z.* **1934**, *68*, 2−15. (b) Jacobson, H.; Stockmayer, W. H. *J. Chem. Phys.* **1950**, *18*, 1600−1606. (c) Flory, P. J.; Suter, U. W.; Mutter, M. *J. Am. Chem. Soc.* **1976**, *98*, 5733−5739. (d) Jencks, W. P. *Proc. Natl. Acad. Sci. U.S.A.* **1981**, *78*, 4046−4050. (e) Winnik, M. A. *Chem. Rev.* **1981**, *81*, 491−524. (f) Chi, X.; Guerin, A. J.; Haycock, R. A.; Hunter, C. A.; Sarson, L. D. *J. Chem. Soc., Chem. Commun.* **1995**, 2563−2565. (g) Ercolani, G. *J. Phys. Chem. B* **1998**, *102*, 5699−5703. (h) Kramer, R. H.; Karpen, J. W. *Nature* **1998**, *395*, 710−713. (i) Galli, C.; Mandolini, L. *Eur. J. Org. Chem.* **2000**, 3117−3125. (j) Gargano, J. M.; Ngo, T.; Kim, J. Y.; Acheson, D. W. K.; Lees, W. J. *J. Am. Chem. Soc.* **2001**, *123*, 12909−12910.

(24) André, N.; Jensen, T. B.; Scopelliti, R.; Imbert, D.; Elhabiri, M.; Hopfgartner, G.; Piguet, C.; Bünzli, J.-C. G. *Inorg. Chem.* **2004**, *43*, 515−529.

(25) Willcott, M. R.; Lenkinski, R. E.; Davis, R. E. *J. Am. Chem. Soc.* **1972**, *94*, 1742−1744.

(26) (a) Choppin, G. R. In *Lanthanide Probes in Life, Chemical and Earth Sciences*; Elsevier: Amsterdam, The Netherlands, 1989; Chapter 1. (b) Piguet, C.; Bünzli, J.-C. G. *Chem. Soc. Rev.* **1999**, *28*, 347−358. (c) Comuzzi, C.; Di Bernardo, P.; Portanova, R.; Tolazzi, M.; Zanonato, P. L. *Polyhedron* **2002**, *21*, 1385−1391. (d) Di Bernardo, P.; Melchior, A.; Tolazzi, M.; Zanonato, P. L. *Coord. Chem. Rev.* **2012**, *256*, 328−351.

(27) According to Kuhn's theory, the entropic part of *EM* depends on (i) the distance between the two interacting sites and (ii) the average length of the chain connecting these sites.[23] Since these parameters do not depend on the selected lanthanides, we assume identical entropic contributions to *EM* in $[Ln_2(\mathbf{L9})]^{6+}$.

(28) Le Borgne, T.; Altmann, P.; André, N.; Bünzli, J.-C. G.; Bernardinelli, G.; Morgantini, P.-Y.; Weber, J.; Piguet, C. *Dalton Trans.* **2004**, 723−733.

(29) (a) Jensen, T. B.; Scopelliti, R.; Bünzli, J.-C. G. *Inorg. Chem.* **2006**, *45*, 7806−7814. (b) Jensen, T. B.; Scopelliti, R.; Bünzli, J.-C. G. *Chem.—Eur. J.* **2007**, *13*, 8404−8410.

(30) Piguet, C.; Bünzli, J.-C. G. In *Handbook on the Physics and Chemistry of Rare Earths*; GschneidnerJr, K. A., Bünzli, J.-C. G., Pecharsky, V. K., Eds.; Elsevier Science: Amsterdam, The Netherlands, 2009; Vol. *40*, pp 301−553.

(31) Borkovec, M.; Hamacek, J.; Piguet, C. *Dalton Trans.* **2004**, 4096−4105.

(32) Dalla Favera, N.; Hamacek, J.; Borkovec, M.; Jeannerat, D.; Ercolani, G.; Piguet, C. *Inorg. Chem.* **2007**, *46*, 9312−9322.

(33) (a) Perlmutter-Hayman, B. *Acc. Chem. Res.* **1986**, *19*, 90−96. (b) Borkovec, M.; Koper, G. J. M.; Piguet, C. *Curr. Opin. Colloid Interface Sci.* **2006**, *11*, 280−289. (c) Thordarson, P. *Chem. Soc. Rev.* **2011**, *40*, 1305−1323. (d) Borkovec, M.; Cakara, D.; Koper, G. J. M. *J. Phys. Chem. B* **2012**, *116*, 4300−4309.

(34) Ercolani, G.; Schiaffino, L. *Angew. Chem., Int. Ed.* **2011**, *50*, 1762−1768.
(35) (a) Libman, J.; Tor, Y.; Shanzer, A. *J. Am. Chem. Soc.* **1987**, *109*, 5880−5881. (b) Blanc, S.; Yakirevich, P.; Leize, E.; Meyer, M.; Libman, J.; Van Dorsselaer, A.; Albrecht-Gary, A.-M.; Shanzer, A. *J. Am. Chem. Soc.* **1997**, *119*, 4934−4944.
(36) (a) Riis-Johannessen, T.; Dalla Favera, N.; Todorova, T. K.; Huber, S. M.; Gagliardi, L.; Piguet, C. *Chem.—Eur. J.* **2009**, *15*, 12702−12718. (b) Dalla Favera, N.; Kiehne, U.; Bunzen, J.; Hyteballe, S.; Lützen, A.; Piguet, C. *Angew. Chem., Int. Ed.* **2010**, *49*, 125−128.
(37) (a) Bünzli, J.-C. G. *Chem. Rev.* **2010**, *110*, 2729−2755. (b) Eliseeva, S. V.; Bünzli, J.-C. G. *New J. Chem.* **2011**, *35*, 1165−1176. (c) Aboshyan-Sorgho, L.; Cantuel, M.; Petoud, S.; Hauser, A.; Piguet, C. *Coord. Chem. Rev.* **2012**, *256*, 1644−1663.
(38) Senegas, J.-M.; Koeller, S.; Bernardinelli, G.; Piguet, C. *Chem. Commun.* **2005**, 2235−2237.
(39) Johansen, J. E.; Christie, B. D.; Rapoport, H. *J. Org. Chem.* **1981**, *46*, 4914−4920.
(40) Piguet, C.; Bernardinelli, G.; Bocquet, B.; Quattropanni, A.; Williams, A. F. *J. Am. Chem. Soc.* **1992**, *114*, 7440−7451.
(41) Piguet, C.; Bocquet, B.; Hopfgartner, G. *Helv. Chim. Acta* **1994**, *77*, 931−942.
(42) Desreux, J. F. In *Lanthanide Probes in Life, Chemical and Earth Sciences*; Bünzli, J.-C. G., Choppin, G. R., Eds.; Elsevier: Amsterdam, The Netherlands, 1989; Chapter 2, p 43.
(43) Malinowski, E. R.; Howery, D. G. *Factor Analysis in Chemistry*; Wiley: New York, 1980.

Allosteric effects in Binuclear Homo- and Hetero-metallic Triple-Stranded Lanthanide Podates.

Patrick E. Ryan, Gabriel Canard,[*] Sylvain Koeller, Bernard Bocquet and Claude Piguet[*]

Supporting Information

(13 pages)

Table S1 ^{1}H NMR Chemical Shifts in **L9** and $[Ln_2(\mathbf{L9})]^{6+}$ (Ln = La, Eu, Lu) in CD_3CN at 298 K.[a]

	L9	$[La_2(\mathbf{L9})]^{6+}$	$[Lu_2(\mathbf{L9})]^{6+}$		**L9**	$[La_2(\mathbf{L9})]^{6+}$	$[Lu_2(\mathbf{L9})]^{6+}$
H1	0.75	0.32	0.36	H16	7.24	7.02	6.94
H2	1.41	0.20	0.25	H17	7.36	7.19	7.25
H3	2.27	0.85	0.90	H18	8.37	8.30	8.38
		1.25	1.22				
H4	3.80	2.74	2.60	H19	7.91	8.30	8.25
		3.44	3.34				
H5	7.72	6.18	5.97	H20	7.53	7.72	7.59
H6	7.29	7.30	7.31	H21	4.73	4.31	4.36
						4.45	4.52
H7	7.36	7.64	7.65	H22	1.29	1.51	1.50
H8	8.29	7.64	7.65	H23	4.73	4.18	4.28
						4.45	4.52
H9	7.97	8.11	7.92	H24	1.29	1.23	1.04
H10	8.29	7.92	7.73	H25	4.73	4.45	4.61
						4.69	4.78
H11	7.36	7.72	7.73	H26	1.41	1.51	1.50
H12	7.24	7.37	7.31	H27	3.34	2.72	2.63
						2.81	2.75
H13	7.72	5.96	5.44	H28	1.06	0.71	0.62
H14	4.28	3.54	3.50	H29	3.60	3.24	3.27
		3.71	3.62			3.35	3.40
H15	7.69	5.98	5.46	H30	1.29	0.78	0.62

[a] Numbering is shown in scheme 1.

Table S2 ESI-MS Titrations of **L9** with $La(CF_3SO_3)_3 \cdot H_2O$ in CH_3CN/CH_2Cl_2 (9:1).[a]

	m/z exp.	Intensity [b]
$\lvert La\rvert_{tot} / \lvert \mathbf{L9}\rvert_{tot} = 1$		
$[H_2\mathbf{L9}]^{2+}$	1177.0	vw
$[La(\mathbf{L9})]^{3+}$	830.5	vs
$[La(\mathbf{L9})(CF_3SO_3)]^{2+}$	1319.8	w
$\lvert La\rvert_{tot} / \lvert \mathbf{L9}\rvert_{tot} = 2$		
$[La(\mathbf{L9})]^{3+}$	830.5	s
$[La(\mathbf{L9})(CF_3SO_3)]^{2+}$	1320.0	w
$[La_2(\mathbf{L9})]^{6+}$	438.4	w
$[La_2(\mathbf{L9})(CF_3SO_3)_2]^{4+}$	732.1	s
$[La_2(\mathbf{L9})(CF_3SO_3)_3]^{3+}$	1025.6	w
$[La_2(\mathbf{L9})(CF_3SO_3)_4]^{2+}$	1613.9	vw
$\lvert La\rvert_{tot} / \lvert \mathbf{L9}\rvert_{tot} = 3$		
$[La_2(\mathbf{L9})]^{6+}$	438.4	vs
$[La_2(\mathbf{L9})(CF_3SO_3)_2]^{4+}$	732.0	vs
$[La_2(\mathbf{L9})(CF_3SO_3)_3]^{3+}$	1025.5	vs
$[La_2(\mathbf{L9})(CF_3SO_3)_4]^{2+}$	1613.0	w

[a] $\lvert \mathbf{L9}\rvert_{tot} = 2 \cdot 10^{-4}$ M. [b] w = weak, s = strong, v = very.

Table S3 ESI-MS Titrations of **L9** with $Eu(CF_3SO_3)_3 \cdot 2H_2O$ in CH_3CN/CH_2Cl_2 (9:1).[a]

	m/z exp.	Intensity [b]
$\lvert Eu\rvert_{tot} / \lvert \mathbf{L9}\rvert_{tot} = 1$		
$[H_2\mathbf{L9}]^{2+}$	1176.8	vs
$[Eu(\mathbf{L9})]^{3+}$	835.0	vs
$[Eu(\mathbf{L9})(CF_3SO_3)]^{2+}$	1326.7	s
$[Eu_2(\mathbf{L9})(CF_3SO_3)_3]^{3+}$	1034.2	s
$[Eu_2(\mathbf{L9})(CF_3SO_3)_4]^{2+}$	1624.7	vw
$\lvert Eu\rvert_{tot} / \lvert \mathbf{L9}\rvert_{tot} = 2$		
$[Eu(\mathbf{L9})]^{3+}$	834.7	vw
$[Eu_2(\mathbf{L9})(CF_3SO_3)_2]^{4+}$	738.8	s
$[Eu_2(\mathbf{L9})(CF_3SO_3)_3]^{3+}$	1034.2	vs
$[Eu_2(\mathbf{L9})(CF_3SO_3)_4]^{2+}$	1625.9	vw
$\lvert Eu\rvert_{tot} / \lvert \mathbf{L9}\rvert_{tot} = 3$		
$[Eu_2(\mathbf{L9})]^{6+}$	442.8	vs
$[Eu_2(\mathbf{L9})(CF_3SO_3)]^{5+}$	561.2	w
$[Eu_2(\mathbf{L9})(CF_3SO_3)_2]^{4+}$	738.8	vs
$[Eu_2(\mathbf{L9})(CF_3SO_3)_3]^{3+}$	1034.6	s
$[Eu_2(\mathbf{L9})(CF_3SO_3)_4]^{2+}$	1626.4	vw

[a] $\lvert \mathbf{L9}\rvert_{tot} = 2 \cdot 10^{-4}$ M. [b] w = weak, s = strong, v = very.

Table S4 ESI-MS Titrations of **L9** with $Lu(CF_3SO_3)_3 \cdot H_2O$ in CH_3CN/CH_2Cl_2 (9:1).[a]

	m/z exp.	Intensity [b]
$\|Lu\|_{tot} / \|\mathbf{L9}\|_{tot} = 1$		
$[H_2\mathbf{L9}]^{2+}$	1177.3	vs
$[Lu(\mathbf{L9})]^{3+}$	842.4	vs
$[Lu_2(\mathbf{L9})(CF_3SO_3)_3]^{3+}$	1049.6	vw
$\|Lu\|_{tot} / \|\mathbf{L9}\|_{tot} = 2$		
$[Lu(\mathbf{L9})]^{3+}$	842.5	vw
$[Lu(\mathbf{L9})(CF_3SO_3)]^{2+}$	1338.0	vw
$[Lu_2(\mathbf{L9})]^{6+}$	450.5	vs
$[Lu_2(\mathbf{L9})(CF_3SO_3)]^{5+}$	570.4	s
$[Lu_2(\mathbf{L9})(CF_3SO_3)_2]^{4+}$	750.1	vs
$[Lu_2(\mathbf{L9})(CF_3SO_3)_3]^{3+}$	1049.8	vs
$[Lu_2(\mathbf{L9})(CF_3SO_3)_4]^{2+}$	1648.9	vw
$\|Lu\|_{tot} / \|\mathbf{L9}\|_{tot} = 3$		
$[Lu_2(\mathbf{L9})]^{6+}$	450.5	vw
$[Lu_2(\mathbf{L9})(CF_3SO_3)_2]^{4+}$	750.2	vs
$[Lu_2(\mathbf{L9})(CF_3SO_3)_3]^{3+}$	1049.5	vs
$[Lu_2(\mathbf{L9})(CF_3SO_3)_4]^{2+}$	1649.3	vw

[a] $|\mathbf{L9}|_{tot} = 2 \cdot 10^{-4}$ M. [b] w = weak, s = strong, v = very.

Table S5 Cumulative Experimental and Calculated (eqs 5-6 and S1-S8) Thermodynamic Formation Constants ($\log(\beta_{m,n}^{\mathrm{Ln},\mathbf{Lk}})$) Obtained for $[\mathrm{Ln}_m(\mathbf{Lk})_n]^{3m+}$ in CH_3CN/CH_2Cl_2 (9:1) + 10^{-2} M NBu_4ClO_4 at 298 K (Ln = La, Eu, Lu; **L*k*** = **L7**, **L9**, **L11**, **L12**).

Metal	La		Eu		Lu		Reference
	exptl	calcd	exptl	calcd	exptl	calcd	
$\log(\beta_{1,1}^{\mathrm{Ln},\mathbf{L7}})$	7.39(1)	7.63	8.10(1)	7.89	10.1(4)	10.41	This work
$\log(\beta_{1,2}^{\mathrm{Ln},\mathbf{L7}})$	13.31(2)	13.07	14.22(2)	14.43	18.4(8)	18.09	This work
$\log(\beta_{1,3}^{\mathrm{Ln},\mathbf{L7}})$	17.87(2)	16.59	19.62(2)	19.95	23.9(2)	23.35	This work
$\log(\beta_{1,1}^{\mathrm{Ln},\mathbf{L11}})$	4.55(1)	4.44	8.25(3)	8.77	9.93(9)	9.83	This work
$\log(\beta_{1,2}^{\mathrm{Ln},\mathbf{L11}})$	9.06(1)	9.17	16.25(6)	15.73	17.4(2)	17.50	This work
$\log(\beta_{1,3}^{\mathrm{Ln},\mathbf{L11}})$	13.19(1)	14.51	21.38(7)	21.16	22.7(2)	23.32	This work
$\log(\beta_{1,1}^{\mathrm{Ln},\mathbf{L12}})$	8.2(2)	6.84	7.7(4)	7.79	7.9(3)	7.13	10b
$\log(\beta_{1,1}^{\mathrm{Ln},\mathbf{L8}})$	7.6(2)	8.92	7.2(1)	6.57	8.0(1)	7.15	11
$\log(\beta_{1,1}^{\mathrm{Ln},\mathbf{L9}})$	8.89(4)	8.92	6.41(9)	6.95	5.57(1)	7.19	This work
$\log(\beta_{2,1}^{\mathrm{Ln},\mathbf{L9}})$	15.47(5)	15.47	12.80(8)	12.80	10.82(1)	10.82	This work
AF_{Ln} [a]	0.075		0.029		0.047		

[a] Wilcott Agreement Factor $AF_{\mathrm{Ln}} = \sqrt{\sum_i \left(\log\left(\beta_{m,n,\mathrm{exptl}}^{\mathrm{Ln},\mathbf{Lk}}\right) - \log\left(\beta_{m,n,\mathrm{calcd}}^{\mathrm{Ln},\mathbf{Lk}}\right)\right)^2 / \sum_i \left(\log\left(\beta_{m,n,\mathrm{exp}}^{\mathrm{Ln},\mathbf{Lk}}\right)\right)^2}$.[25]

a)

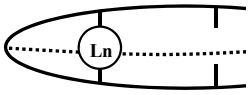

$$[Ln(CH_3CN)_9]^{3+} + \mathbf{L9} \rightleftharpoons \underset{\beta_{1,1,N3}^{Ln,\mathbf{L9}}}{} \textit{proximal}\text{-}[Ln(\mathbf{L9})]^{3+} + 9\,CH_3CN \quad (1a)$$

Point groups:	D_{3h}	C_{3v}	C_3	C_{3v}
σ^{ext}:	6	3	3	3
σ^{int}:	3^9	3^{16}	3^{16}	1
σ^{chiral}:	1	1	1/2	1

$$\omega_{1,1,N3}^{chiral}\omega_{1,1,N3}^{Ln,\mathbf{L9}} = \frac{\left(6\cdot 3^9\cdot 1\right)\cdot\left(3\cdot 3^{16}\cdot 1\right)}{\left(3\cdot 3^{16}\cdot 1/2\right)\cdot\left(3\cdot 1\cdot 1\right)^9} = 12$$

$$\Rightarrow \beta_{1,1,N3}^{Ln,\mathbf{L9}} = 12\left(f_{N3}^{Ln}\right)^3\left(EM_{prox}^{Ln}\right)^2\left(u_{Ln}^{N3,N3}\right)^3 \quad (3a)$$

b)

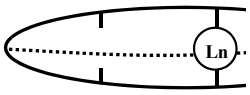

$$[Ln(CH_3CN)_9]^{3+} + \mathbf{L9} \rightleftharpoons \underset{\beta_{1,1,N2O}^{Ln,\mathbf{L9}}}{} \textit{distal}\text{-}[Ln(\mathbf{L9})]^{3+} + 9\,CH_3CN \quad (1b)$$

Point groups:	D_{3h}	C_{3v}	C_3	C_{3v}
σ^{ext}:	6	3	3	3
σ^{int}:	3^9	3^{16}	3^{16}	1
σ^{chiral}:	1	1	1/2	1

$$\omega_{1,1,N2O}^{chiral}\omega_{1,1,N2O}^{Ln,\mathbf{L9}} = \frac{\left(6\cdot 3^9\cdot 1\right)\cdot\left(3\cdot 3^{16}\cdot 1\right)}{\left(3\cdot 3^{16}\cdot 1/2\right)\cdot\left(3\cdot 1\cdot 1\right)^9} = 12$$

$$\Rightarrow \beta_{1,1,N2O}^{Ln,\mathbf{L9}} = 12\left(f_{N2O}^{Ln}\right)^3\left(EM_{dist}^{Ln}\right)^2\left(u_{Ln}^{N2O,N2O}\right)^3 \quad (3b)$$

c)

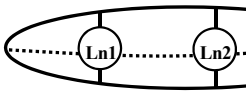

$$2\,[Ln(CH_3CN)_9]^{3+} + \mathbf{L9} \rightleftharpoons \underset{\beta_{2,1}^{Ln,\mathbf{L9}}}{} [Ln_2(\mathbf{L9})]^{6+} + 18\,CH_3CN \quad (2)$$

Point groups:	D_{3h}	C_{3v}	C_3	C_{3v}
σ^{ext}:	6	3	3	3
σ^{int}:	3^9	3^{16}	3^{16}	1
σ^{chiral}:	1	1	1/2	1

$$\omega_{2,1}^{chiral}\omega_{2,1}^{Ln,\mathbf{L9}} = \frac{\left(6\cdot 3^9\cdot 1\right)^2\cdot\left(3\cdot 3^{16}\cdot 1\right)}{\left(3\cdot 3^{16}\cdot 1/2\right)\cdot\left(3\cdot 1\cdot 1\right)^{18}} = 72$$

$$\Rightarrow \beta_{2,1}^{Ln,\mathbf{L9}} = 72\left(f_{N3}^{Ln}\right)^3\left(f_{N2O}^{Ln}\right)^3\left(EM_{prox}^{Ln}\right)^2\left(EM_{dist\text{-}n}^{Ln}\right)^2\left(u_{Ln}^{N3,N3}\right)^3\left(u_{Ln}^{N2O,N2O}\right)^3\left(u^{Ln,Ln}\right) \quad (4)$$

Figure S1 Application of the site binding model[18] showing the determination of symmetry numbers (σ^{ext}, σ^{int}, σ^{chiral})[20] for the microspecies $[Ln_m(\mathbf{L9})]^{3m+}$ contributing to equilibria (1)-(2).

a) 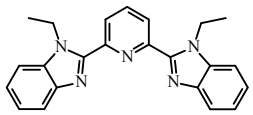

$$[Ln(CH_3CN)_9]^{3+} + \mathbf{L7} \rightleftharpoons [Ln(\mathbf{L7})(CH_3CN)_6]^{3+} + 3\,CH_3CN \quad (7.1)$$

$\beta_{1,1}^{Ln,\mathbf{L7}}$

Point groups:	D_{3h}	C_{2v}	C_{2v}	C_{3v}
σ^{ext}:	6	2	2	3
σ^{int}:	3^9	3^2	3^8	1
σ^{chiral}:	1	1	1	1

$$\omega_{1,1}^{chiral}\omega_{1,1}^{Ln,\mathbf{L7}} = \frac{\left(6\cdot 3^9\cdot 1\right)\cdot\left(2\cdot 3^2\cdot 1\right)}{\left(2\cdot 3^8\cdot 1\right)\cdot\left(3\cdot 1\cdot 1\right)^3} = 6$$

$$\Rightarrow \beta_{1,1}^{Ln,\mathbf{L7}} = 6\left(f_{N3}^{Ln}\right) \quad (S1)$$

b) $$[Ln(CH_3CN)_9]^{3+} + 2\,\mathbf{L7} \rightleftharpoons [Ln(\mathbf{L7})_2(CH_3CN)_3]^{3+} + 6\,CH_3CN \quad (7.2)$$

$\beta_{1,2}^{Ln,\mathbf{L7}}$

Point groups:	D_{3h}	C_{2v}	C_{2v}	C_{3v}
σ^{ext}:	6	2	2	3
σ^{int}:	3^9	3^2	3^7	1
σ^{chiral}:	1	1	1	1

$$\omega_{1,2}^{chiral}\omega_{1,2}^{Ln,\mathbf{L7}} = \frac{\left(6\cdot 3^9\cdot 1\right)\cdot\left(2\cdot 3^2\cdot 1\right)^2}{\left(2\cdot 3^7\cdot 1\right)\cdot\left(3\cdot 1\cdot 1\right)^6} = 12$$

$$\Rightarrow \beta_{1,2}^{Ln,\mathbf{L7}} = 12\left(f_{N3}^{Ln}\right)^2\left(u_{Ln}^{N3,N3}\right) \quad (S2)$$

c) $$[Ln(CH_3CN)_9]^{3+} + 3\,\mathbf{L7} \rightleftharpoons [Ln(\mathbf{L7})_3]^{3+} + 9\,CH_3CN \quad (7.3)$$

$\beta_{1,3}^{Ln,\mathbf{L7}}$

Point groups:	D_{3h}	C_{2v}	D_3	C_{3v}
σ^{ext}:	6	2	6	3
σ^{int}:	3^9	3^2	3^6	1
σ^{chiral}:	1	1	1/2	1

$$\omega_{1,3}^{chiral}\omega_{1,3}^{Ln,\mathbf{L7}} = \frac{\left(6\cdot 3^9\cdot 1\right)\cdot\left(2\cdot 3^2\cdot 1\right)^3}{\left(6\cdot 3^6\cdot 1/2\right)\cdot\left(3\cdot 1\cdot 1\right)^9} = 16$$

$$\Rightarrow \beta_{1,3}^{Ln,\mathbf{L7}} = 16\left(f_{N3}^{Ln}\right)^3\left(u_{Ln}^{N3,N3}\right)^3 \quad (S3)$$

Figure S2 Application of the site binding model[18] showing the determination of symmetry numbers (σ^{ext}, σ^{int}, σ^{chiral})[20] for the microspecies $[Ln(\mathbf{L7})_n]^{3+}$ contributing to equilibria (7).

a) 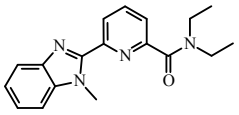

$$[Ln(CH_3CN)_9]^{3+} + \mathbf{L11} \underset{}{\overset{\beta_{1,1}^{Ln,\mathbf{L11}}}{\rightleftharpoons}} [Ln(\mathbf{L11})(CH_3CN)_6]^{3+} + 3\,CH_3CN \quad (7.4)$$

Point groups:	D_{3h}	C_s	C_s	C_{3v}
σ^{ext}:	6	1	1	3
σ^{int}:	3^9	3^3	3^9	1
σ^{chiral}:	1	1	1	1

$$\omega_{1,1}^{chiral}\omega_{1,1}^{Ln,\mathbf{L11}} = \frac{\left(6\cdot 3^9\cdot 1\right)\cdot\left(1\cdot 3^3\cdot 1\right)}{\left(1\cdot 3^9\cdot 1\right)\cdot\left(3\cdot 1\cdot 1\right)^3} = 6$$

$$\Rightarrow \beta_{1,1}^{Ln,\mathbf{L11}} = 6\left(f_{N2O}^{Ln}\right) \quad (S4)$$

b) $$[Ln(CH_3CN)_9]^{3+} + 2\,\mathbf{L11} \underset{}{\overset{\beta_{1,2}^{Ln,\mathbf{L11}}(HH)}{\rightleftharpoons}} HH\text{-}[Ln(\mathbf{L11})_2(CH_3CN)_3]^{3+} + 6\,CH_3CN \quad (7.5a)$$

Point groups:	D_{3h}	C_s	C_s	C_{3v}
σ^{ext}:	6	1	1	3
σ^{int}:	3^9	3^3	3^9	1
σ^{chiral}:	1	1	1	1

$$\omega_{1,2}^{chiral}\omega_{1,2}^{Ln,\mathbf{L11}}(HH) = \frac{\left(6\cdot 3^9\cdot 1\right)\cdot\left(1\cdot 3^3\cdot 1\right)^2}{\left(1\cdot 3^9\cdot 1\right)\cdot\left(3\cdot 1\cdot 1\right)^6} = 6$$

$$\Rightarrow \beta_{1,2}^{Ln,\mathbf{L11}}(HH) = 6\left(f_{N2O}^{Ln}\right)^2\left(u_{Ln}^{N2O,N2O}(HH)\right) \quad (S5a)$$

c) $$[Ln(CH_3CN)_9]^{3+} + 2\,\mathbf{L11} \underset{}{\overset{\beta_{1,2}^{Ln,\mathbf{L11}}(HT)}{\rightleftharpoons}} HT\text{-}[Ln(\mathbf{L11})_2(CH_3CN)_3]^{3+} + 6\,CH_3CN \quad (7.5b)$$

Point groups:	D_{3h}	C_s	C_2	C_{3v}
σ^{ext}:	6	1	2	3
σ^{int}:	3^9	3^3	3^9	1
σ^{chiral}:	1	1	1/2	1

$$\omega_{1,2}^{chiral}\omega_{1,2}^{Ln,\mathbf{L11}}(HT) = \frac{\left(6\cdot 3^9\cdot 1\right)\cdot\left(1\cdot 3^3\cdot 1\right)^2}{\left(2\cdot 3^9\cdot 1/2\right)\cdot\left(3\cdot 1\cdot 1\right)^6} = 6$$

$$\Rightarrow \beta_{1,2}^{Ln,\mathbf{L11}}(HT) = 6\left(f_{N2O}^{Ln}\right)^2\left(u_{Ln}^{N2O,N2O}(HT)\right) \quad (S5b)$$

Assuming $u_{Ln}^{N2O,N2O}(HH) \approx u_{Ln}^{N2O,N2O}(HT) \quad \Rightarrow \beta_{1,2}^{Ln,\mathbf{L11}} = 12\left(f_{N2O}^{Ln}\right)^2\left(u_{Ln}^{N2O,N2O}\right)$ (S5)

d) 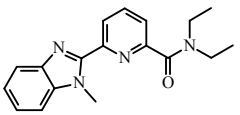

$$[Ln(CH_3CN)_9]^{3+} + 3\,\mathbf{L11} \rightleftharpoons \textit{HHH}\text{-}[Ln(\mathbf{L11})_3]^{3+} + 9\,CH_3CN \quad (7.6a)$$

$\beta_{1,3}^{Ln,\mathbf{L11}}(HHH)$

Point groups:	D_{3h}	C_s	C_3	C_{3v}
σ^{ext}:	6	1	3	3
σ^{int}:	3^9	3^3	3^9	1
σ^{chiral}:	1	1	1/2	1

$$\omega_{1,3}^{chiral}\omega_{1,3}^{Ln,\mathbf{L11}}(HHH) = \frac{\left(6\cdot 3^9\cdot 1\right)\cdot\left(1\cdot 3^3\cdot 1\right)^3}{\left(3\cdot 3^9\cdot 1/2\right)\cdot\left(3\cdot 1\cdot 1\right)^9} = 4$$

$$\Rightarrow \beta_{1,3}^{Ln,\mathbf{L11}}(HHH) = 4\left(f_{N2O}^{Ln}\right)^3\left(u_{Ln}^{N2O,N2O}(HH)\right)^3 \quad (S6a)$$

e) $$[Ln(CH_3CN)_9]^{3+} + 3\,\mathbf{L11} \rightleftharpoons \textit{HHT}\text{-}[Ln(\mathbf{L11})_3]^{3+} + 9\,CH_3CN \quad (7.6b)$$

$\beta_{1,3}^{Ln,\mathbf{L11}}(HHT)$

Point groups:	D_{3h}	C_s	C_1	C_{3v}
σ^{ext}:	6	1	1	3
σ^{int}:	3^9	3^3	3^9	1
σ^{chiral}:	1	1	1/2	1

$$\omega_{1,3}^{chiral}\omega_{1,3}^{Ln,\mathbf{L11}}(HHT) = \frac{\left(6\cdot 3^9\cdot 1\right)\cdot\left(1\cdot 3^3\cdot 1\right)^3}{\left(1\cdot 3^9\cdot 1/2\right)\cdot\left(3\cdot 1\cdot 1\right)^9} = 12$$

$$\Rightarrow \beta_{1,3}^{Ln,\mathbf{L11}}(HHT) = 12\left(f_{N2O}^{Ln}\right)^3\left(u_{Ln}^{N2O,N2O}(HT)\right)^3 \quad (S6b)$$

Assuming $u_{Ln}^{N2O,N2O}(HH) \approx u_{Ln}^{N2O,N2O}(HT) \quad \Rightarrow \beta_{1,3}^{Ln,\mathbf{L11}} = 16\left(f_{N2O}^{Ln}\right)^3\left(u_{Ln}^{N2O,N2O}\right)^3 \quad (S6)$

Figure S3 Application of the site binding model[18] showing the determination of symmetry numbers (σ^{ext}, σ^{int}, σ^{chiral})[20] for the microspecies $[Ln(\mathbf{L11})_n]^{3+}$ contributing to equilibria (7).

a)

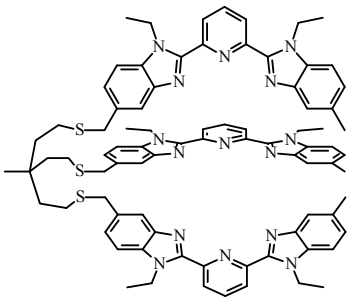

$$[Ln(CH_3CN)_9]^{3+} + \mathbf{L8} \rightleftharpoons[\beta_{1,1}^{Ln,\mathbf{L8}}] [Ln(\mathbf{L8})]^{3+} + 9\,CH_3CN \quad (8.1)$$

Point groups:	D_{3h}	C_{3v}	C_3	C_{3v}
σ^{ext}:	6	3	3	3
σ^{int}:	3^9	3^{10}	3^{10}	1
σ^{chiral}:	1	1	1/2	1

$$\omega_{1,1}^{chiral}\omega_{1,1}^{Ln,\mathbf{L8}} = \frac{\left(6\cdot 3^9\cdot 1\right)\cdot\left(3\cdot 3^{10}\cdot 1\right)}{\left(3\cdot 3^{10}\cdot 1/2\right)\cdot\left(3\cdot 1\cdot 1\right)^9} = 12$$

$$\Rightarrow \beta_{1,1}^{Ln,\mathbf{L8}} = 12\left(f_{N3}^{Ln}\right)^3\left(EM_{prox}^{Ln}\right)^2\left(u_{Ln}^{N3,N3}\right)^3 \quad (S7)$$

b)

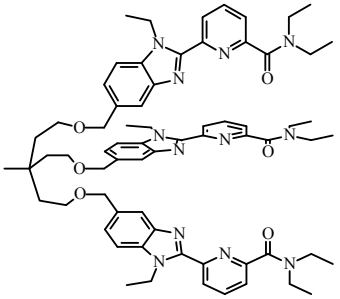

$$[Ln(CH_3CN)_9]^{3+} + \mathbf{L12} \rightleftharpoons[\beta_{1,1}^{Ln,\mathbf{L12}}] [Ln(\mathbf{L12})]^{3+} + 9\,CH_3CN \quad (8.2)$$

Point groups:	D_{3h}	C_{3v}	C_3	C_{3v}
σ^{ext}:	6	3	3	3
σ^{int}:	3^9	3^{10}	3^{10}	1
σ^{chiral}:	1	1	1/2	1

$$\omega_{1,1}^{chiral}\omega_{1,1}^{Ln,\mathbf{L12}} = \frac{\left(6\cdot 3^9\cdot 1\right)\cdot\left(3\cdot 3^{10}\cdot 1\right)}{\left(3\cdot 3^{10}\cdot 1/2\right)\cdot\left(3\cdot 1\cdot 1\right)^9} = 12$$

$$\Rightarrow \beta_{1,1}^{Ln,\mathbf{L12}} = 12\left(f_{N2O}^{Ln}\right)^3\left(EM_{prox}^{Ln}\right)^2\left(u_{Ln}^{N2O,N2O}\right)^3 \quad (S8)$$

Figure S4 Application of the site binding model[18] showing the determination of symmetry numbers (σ^{ext}, σ^{int}, σ^{chiral})[20] for the microspecies $[Ln(\mathbf{L}k)]^{3+}$ (k = 8, 12) contributing to equilibria (8).

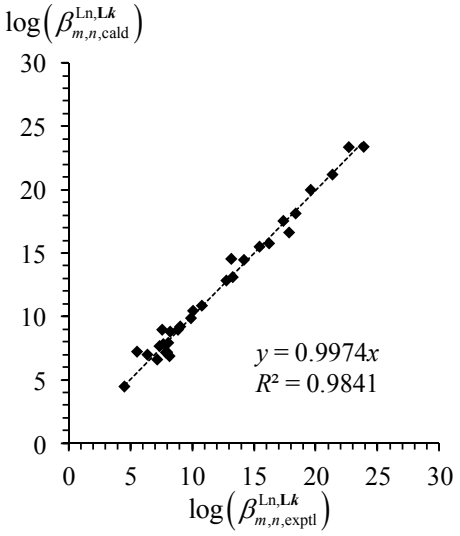

Figure S5 Cumulative experimental ($\log\left(\beta^{\mathrm{Ln,L}k}_{m,n,\mathrm{exptl}}\right)$) and calculated ($\log\left(\beta^{\mathrm{Ln,L}k}_{m,n,\mathrm{calcd}}\right)$, eqns 5-6 and S1-S8) thermodynamic formation constants obtained for $[\mathrm{Ln}_m(\mathbf{L}k)_n]^{3m+}$ in CH_3CN/CH_2Cl_2 (9:1) + 10^{-2} M NBu_4ClO_4 at 298 K (Ln = La, Eu, Lu; **L*k*** = **L7**, **L9**, **L11**, **L12**).

a)

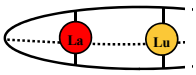

$$[\mathrm{La(CH_3CN)_9}]^{3+} + [\mathrm{Lu(CH_3CN)_9}]^{3+} + \mathbf{L9} \rightleftharpoons [\mathrm{LaLu}(\mathbf{L9})]^{6+} + 18\,\mathrm{CH_3CN} \quad \text{(S9)}$$

$\beta^{\mathrm{La,Lu,L9}}_{1,1,1}$

Point groups:	D_{3h}	D_{3h}	C_{3v}	C_3	C_{3v}
σ^{ext}:	6	6	3	3	3
σ^{int}:	3^9	3^9	3^{16}	3^{16}	1
σ^{chiral}:	1	1	1	1/2	1

$$\omega^{\mathrm{chiral}}_{1,1,1}\omega^{\mathrm{La,Lu,L9}}_{1,1,1} = \frac{\left(6\cdot 3^9\cdot 1\right)^2\cdot\left(3\cdot 3^{16}\cdot 1\right)}{\left(3\cdot 3^{16}\cdot \tfrac{1}{2}\right)\cdot\left(3\cdot 1\cdot 1\right)^{18}} = 72$$

$$\Rightarrow \beta^{\mathrm{La,Lu,L9}}_{1,1,1} = 72\left(f^{\mathrm{La}}_{\mathrm{N3}}\right)^3\left(f^{\mathrm{Lu}}_{\mathrm{N2O}}\right)^3\left(EM^{\mathrm{La}}_{\mathrm{prox}}\right)^2\left(EM^{\mathrm{Lu}}_{\mathrm{prox}}\right)^2(0.69)^2\left(u^{\mathrm{N3,N3}}_{\mathrm{La}}\right)^3\left(u^{\mathrm{N2O,N2O}}_{\mathrm{Lu}}\right)^3\left(u^{\mathrm{La,Lu}}\right) \quad (9)$$

b)

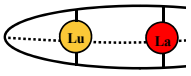

$$[\mathrm{La(CH_3CN)_9}]^{3+} + [\mathrm{Lu(CH_3CN)_9}]^{3+} + \mathbf{L9} \rightleftharpoons [\mathrm{LuLa}(\mathbf{L9})]^{6+} + 18\,\mathrm{CH_3CN} \quad \text{(S10)}$$

$\beta^{\mathrm{Lu,La,L9}}_{1,1,1}$

Point groups:	D_{3h}	D_{3h}	C_{3v}	C_3	C_{3v}
σ^{ext}:	6	6	3	3	3
σ^{int}:	3^9	3^9	3^{16}	3^{16}	1
σ^{chiral}:	1	1	1	1/2	1

$$\omega^{\mathrm{chiral}}_{1,1,1}\omega^{\mathrm{Lu,La,L9}}_{1,1,1} = \frac{\left(6\cdot 3^9\cdot 1\right)^2\cdot\left(3\cdot 3^{16}\cdot 1\right)}{\left(3\cdot 3^{16}\cdot \tfrac{1}{2}\right)\cdot\left(3\cdot 1\cdot 1\right)^{18}} = 72$$

$$\Rightarrow \beta^{\mathrm{Lu,La,L9}}_{1,1,1} = 72\left(f^{\mathrm{Lu}}_{\mathrm{N3}}\right)^3\left(f^{\mathrm{La}}_{\mathrm{N2O}}\right)^3\left(EM^{\mathrm{La}}_{\mathrm{prox}}\right)^2\left(EM^{\mathrm{Lu}}_{\mathrm{prox}}\right)^2(0.69)^2\left(u^{\mathrm{N3,N3}}_{\mathrm{Lu}}\right)^3\left(u^{\mathrm{N2O,N2O}}_{\mathrm{La}}\right)^3\left(u^{\mathrm{Lu,La}}\right) \quad (10)$$

Figure S6 Application of the site binding model[18] showing the determination of symmetry numbers (σ^{ext}, σ^{int}, σ^{chiral})[20] for the microspecies $[\mathrm{LaLu}(\mathbf{L9})]^{6+}$.

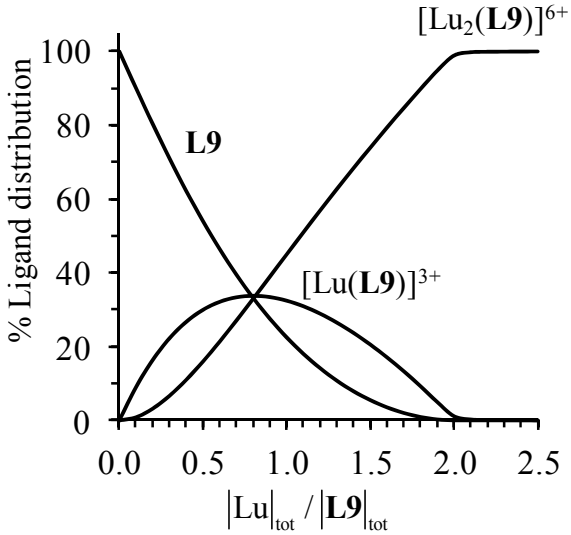

Figure S7 Computed ligand distribution for the titration of **L9** with $Lu(CF_3SO_3)_3$ in CH_3CN/CH_2Cl_2 (9:1) + 10^{-2} M NBu_4ClO_4 at 298 K. Total ligand concentration = 10 mM.